UNIVERSITY OF CALIFORNIA,
IRVINE

Materials and Process Optimization for Performance Enhancement and Cost Reduction for the Packaging of LED Emitters and Solar Cells

DISSERTATION

submitted in partial satisfaction of the requirements
for the degree of

DOCTOR OF PHILOSOPHY

in Materials Science and Engineering

by

Yu-Chou Shih

Dissertation Committee:
Professor Frank G. Shi, Chair
Professor James Earthman
Professor Lizhi Sun

2015

TABLE OF CONTENTS

LIST OF FIGURES

LIST OF TABLES

ACKNOWLEDGMENTS

I would like to express the deepest appreciation to my committee chair, Professor Frank G. Shi, who has the attitude and the substance of a genius: he continually and convincingly conveyed a spirit of adventure in regard to research and scholarship, and an excitement in regard to teaching. Without his guidance, encouragement and persistent help this dissertation would not have been possible.

I would like to thank my committee members, Professor James Earthman, Professor Lizhi Sun, Professor Chin C. Lee and Professor Mikael Nilsson, whose work demonstrated to me that concern for global affairs supported by an "engagement" in comparative literature and modern technology should always transcend academia and provide a quest for our times.

In addition, a thank you to Dr. Jiun-Pyng You, Dr. Nguyen T. Tran, Dr. Yeong-Her Lin, Dr. Bohan Yan, Dr. Yun Shuai and Dr. Ming-Je Sung. As my seniors they provided invaluable help and suggestions on my research, from experiment trainings to technical discussions.

I also thank my junior colleague, Yue Shao, Linguan Huang and Gunwoo Kim, for their help on related experiments.

Special thanks to Yi-San Chang-Yen, Beatrice Mei, Grace Chau, Janine Le and Steve Weinstock at Materials Science Department for helping me through my works.

Last but not least, I would like to thank my family for their unlimited support.

CURRICULUM VITAE

1996-2000 B.E. in Resources Engineering, National Cheng Kung University, Taiwan

2002-2004 M.S. in Materials Science and Engineering, National Chung Hsing University, Taiwan

2009-2010 M.S. in Materials Science and Engineering, University of California, Irvine

2010-2015 Ph.D. in Materials Science and Engineering, University of California, Irvine

FIELD OF STUDY

Optoelectronic Packaging Materials and Technology

PUBLICATIONS

1. Y.C. Shih, Y. Shao and Frank G. Shi, "Novel Non-Glass Frits for Screen-Printable Silicon Solar Cell Metallization," (2015, submitted).

2. Y.C. Shih, F.G. Shi and J.P. You, "Novel Optically Reflective Die Bonding Adhesive for MESA Type Light-Emitting Diodes: Optical and Thermal Performance," (2015, submitted).

3. Y.C. Shih, G.W. Kim, J.P. You and Frank G. Shi, "Light Output Dependence on the Interaction between LED Chip Backside Reflector and Die Attach Adhesives," (2015, submitted).

4. Y. Shao, Y.C. Shih, G.W. Kim and Frank G. Shi, "Study of optimal filler size for high performance polymer-filler composite optical reflectors," *Opt. Mater. Express.*, vol. 5, issue 2, pp. 423-429 (2015).

5. Y.C. Shih, G.W. Kim, L.J. Huang, J.P. You and Frank G. Shi, "Role of Transparent Die Attach Adhesives for Enhancing Lumen Output of Mid-Power LED Emitters with Standard MESA Structure," (2014, accepted by *IEEE Trans. Compon. Packag. Manuf. Tech.*).

6. L.J. Huang, Y.C. Shih and Frank G. Shi, "Effect of Thinning Encapsulant Layer on Junction and Phosphor Temperature of White Light Emitting Diodes," (2014, submitted).

7. Y.C. Shih, Y.H. Lin, J.P. You and Frank G. Shi, "Screen-Printable Silver Pastes with Nanosized Glass Frits for Silicon Solar Cells," *J. Electron. Mater.*, Vol. 42, No. 3, pp. 410-416 (2012).

ABSTRACT OF THE DISSERTATION

Materials and Process Optimization for Performance Enhancement and Cost Reduction for the Packaging of LED Emitters and Solar Cells

By

Yu-Chou Shih

Doctor of Philosophy in Materials Science and Engineering

University of California, Irvine, 2015

Professor Frank G. Shi, Chair

Solar cells and light-emitting diodes (LEDs) are the two most beneficial optoelectronic devices to humanity with opposite functions: one converts photons into electrical power and the other one converts electrons into luminance. Remarkable advances in both applications have been made in both novel chip-level design and packaging technologies, and the continuous innovation and improvement of packaging materials and methods have played key roles in the past two decades. In this work, new packaging materials and technologies are introduced to both silicon solar cells and LEDs to enhance their performance.

The first part of this work was to develop a new silver paste with different glass frits for front-side metallization in silicon solar cells. It is shown that the replacement of micro-sized glass frits by nano-sized ones can dramatically reduce the specific contact resistivity between the resultant silver electrodes and the n-type silicon layer due to the excellent etching ability of nanopartilces on removing the anti-reflection coating (ARC). Surface modification on nano-sized glass frits by electroless plating can further improve the electrical performance by offering extra conducting channel within the insulating layers.

In the second part of this work, the influence of different die attach adhesives (DAAs) on optical and thermal performance of LED emitters was studied. The results show that with an optically clear DAA applied, the highest optical output can be achieved due to its high transparency. The optically reflective DAA also exhibit excellent optical performance, especially at low fillet coverage, which block the photons escaping from the side walls. For high power LED applications, the optically reflective DAA can achieve better thermal management than the conventional one when the bondline thickness is controlled at 7.6 micron.

The last part of this work focuses on the interaction between the LED emitters and the backside reflector, which is used to reflect the downward photons. Our results show that with both optically clear and reflective DAAs, the light output of LED emitters can be very close to that of LED emitters with backside reflectors.

CHAPTER 1

INTRODUCTION

1.1. Background

Optoelectronic devices, such as solar cells, light emitting diodes (LEDs) and laser diodes (LDs), are electronic devices made of semiconductor materials, and they involve the absorption and emission of photons. Optoelectronic devices are based on a versatile structure, the *p-n* junction and perform either electrical-to-optical or optical-to-electrical transduction. Solar cells are used to convert the radiation energy from sunlight into electrical energy for our daily use. On the other hand, LEDs are devices in which the combination of electrons and holes yields photons. There have been significant advances for the two optoelectronic devices in the past two decades and now increasing effort has been put into the research to reduce the manufacturing cost, and to increase the performance and reliability. The focus now is on two aspects: one is the chip-level design and the other one is the packaging technologies. Numerous advances have been introduced into the two optoelectronic devices to improve the overall efficiency, but there are still key issues to be solved for each application [1].

1.2. Solar Cells

Scientists are focusing on three renewable energy technologies, including hydroelectric power, wind power and solar energy. Hydroelectric power brings harm to the local ecosystems and therefore is not considered for new generation of electricity development. Wind power is consistent from long-term duration but shows significant variation over short time scales, and therefore it is used in conjunction with other electricity generating systems to provide a reliable

supply. However this technology requires a broad space and the construction of an electricity grid, it becomes more and more difficult nowadays to find a suitable place for installation of new wind power modules. Solar energy, on the other hand, is an unlimited energy and basically the geological limit (the need for the cooling water) can be neglected. Because it does not introduce huge impact on the environment like the other two technologies do, solar energy is very suitable for household and suburban use [2].

Solar cells or solar photovoltaics are the electronic devices used to collect and covert solar energy into electricity. Solar cells are practical applications of photovoltaic effect, which is related to the photoelectric effect but they have difference processes. Photoelectric effect was first discovered by Heinrich Hertz in 1887. In 1905 Albert Einstein successfully explained this effect by using concepts of photons carrying the light energy. Photoelectric effect is the observation of metals emitting electrons when photons shine upon them. The energy of photons is absorbed by the metal, allowing the electron to be excited from Fermi level to vacuum level. Because most metals possess work function between 3 to 5 eV, only photons with energy in the ultraviolet region could be absorbed by metals to emit electrons. However the ultraviolet region is a small portion in sunlight spectrum, a solar cell made of metals will have efficiency less than 1%. In semiconductors, photovoltaic effect takes place and electrons are excited from valence band to conduction band when absorbing photon energy. The energy gap of III-V semiconductor materials and silicon is about 1 to 2 eV and therefore the materials absorb visible and infrared radiation and the efficiency is much more that metals. So now all solar cells are using semiconductor materials instead of metals.

There are many different types of solar cells, such as crystalline silicon cells, thin-film cells, single- and multi-junction cells, dye-sensitized solar cells (DSSCs) and others. Multi-

junction cells show the highest overall efficiency to date and reached a record of 44% for GaAs-based multi-junction cells. However crystalline silicon cells, whose efficiency is about 24%, are currently dominating the market because they have relative low materials and processing cost per watt. Another reason is that silicon is less toxic compared with other solar cell materials and therefore it is more eco-friendly. Table 1.1 summarized some selected types of second generation solar cells with their advantages and disadvantages. Figure 1.1 shows market share of different types of solar cells from 2011 to 2015 (expected) and the market share of silicon solar cells is 90% in 2014. From this figure it shows that the market is driven by the high-efficiency module technologies, as well as reduction in overall cost.

Table 1.1 Second generation solar cells

	PROs	CONs
Silicon	• Low cost • Suitable for massive production	• Lower efficiency • Lower stability
CIS/CIGS	• Best stability • High efficiency	• Higher cost • Process is not standardized • In and Ga are rare
CdTe	• Highest efficiency • Suitable for massive production	• Highest cost • Cadmium is very toxic • Tellurium is rare
DSSC	• Lowest cost and less materials use • Suitable for large area manufacturing • Processing is easy	• Lowest efficiency • Degradation • Packaging is complex

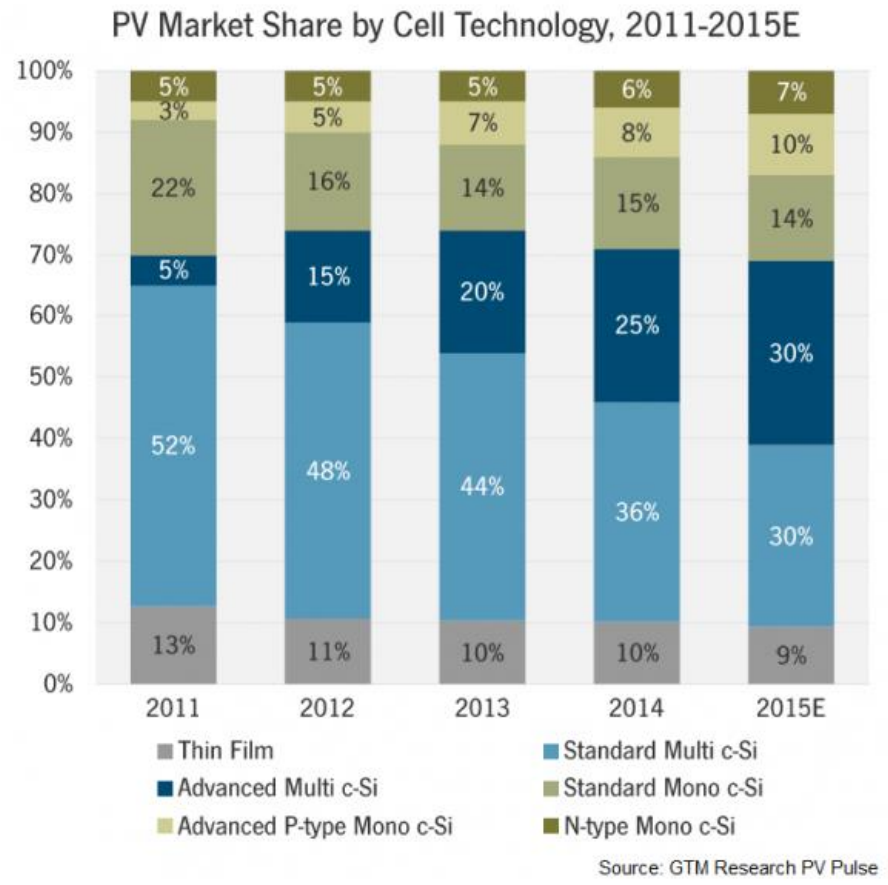

Figure 1.1. Market share of different cell technologies from 2011 to 2015 (expected)

Figure 1.2 shows the illustration of the cross-sectional profile of the *p*-*n* junction in a silicon solar cell. The anti-reflection coating (ARC), typically Si_3N_4, is applied to reduce the escape of photons from the *n*-type silicon layer once photons enter it. However it is electrical isolating and need to be removed so the front silver electrode can make contact with the *n*-type silicon layer and form conducting channel. The *I*-*V* relationship for silicon solar cell can be expressed by the following equation:

$$I = I_s\left(e^{\frac{V-IR_S}{V_T}} - 1\right) + \frac{V-IR_S}{R_{sh}} - I_L \tag{1-1}$$

where *I* is the current, I_s is the saturation current, *V* is the voltage, R_s is the series resistance, R_{sh} is the shunt resistance, I_L is the light generated current, and V_T is a constant, which equals to 0.026V at room temperature. From the equation, if we have a smaller series resistance, R_s, then the current will be larger, which means the overall efficiency will be larger. The resistance at the front silver electrodes and the *n*-type silicon layer is one of the contributions to the series resistance and should be eliminate to attend the maximum efficiency. However the interface resistance is usually high due to the residual glass at the interface and the mechanism is discussed below [2-3].

Screen-printable silver pastes are the packaging components used to form the front electrodes in silicon solar cells. Silver pastes primarily consist of three constituents: (1) metal silver powders, which provide the conductive phase in the resultant films due to its superior conductivity, high chemical stability and lower price among the noble metals; (2) glass frits and oxide additives, which enable and enhance the binding of the silver phase to the silicon substrates and (3) organic phases, which disperse the metallic and ceramic components to impart the desired rheological properties to the pastes. After the pastes are applied onto the ARC layer, the cells will go through a firing step to enable the glass frits and oxide additives to etch through

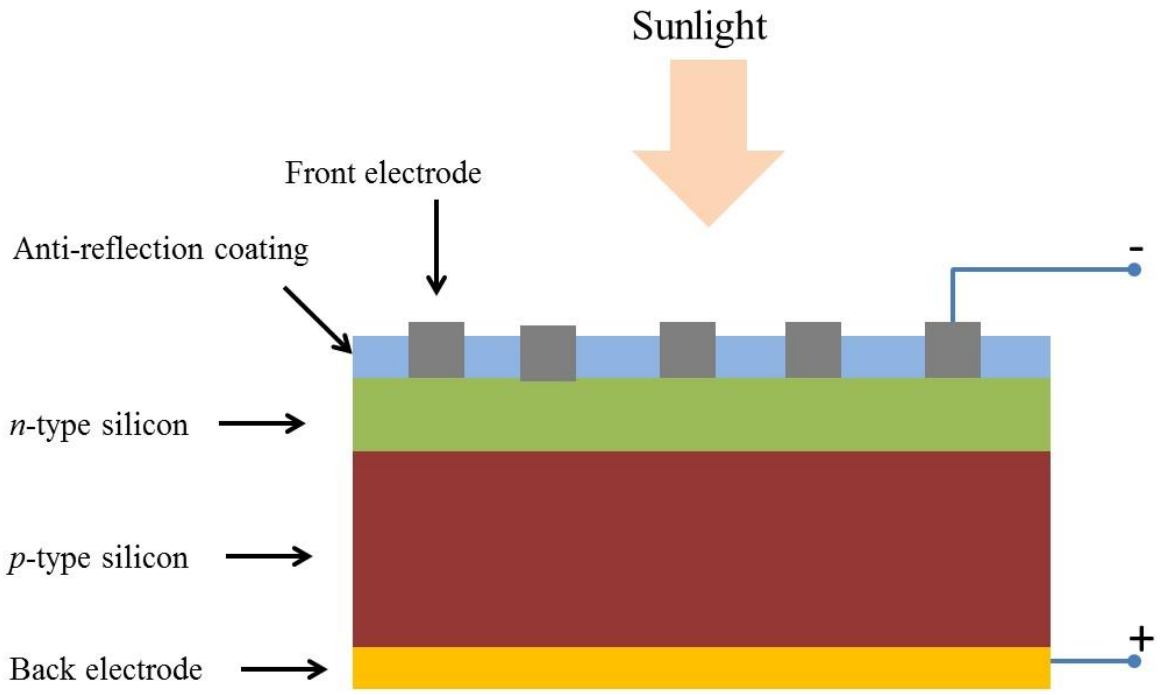

Figure 1.2. The illustration of the cross-sectional profile of the *p*-*n* junction in a silicon solar cell.

the ARC layer so the metallic silver powder can form electrical conductive channels with the underlying *n*-type silicon layer. However there are always residual glass clusters or layers at the silver/silicon boundary, which form electrical isolating region at the interface and increase the contact resistance. The sources of the residual glass the additives that are not reacted during the process and also the composition of the ARC layer. Together they form non-stoichiometric glass compounds at the interfaces. If there are more portions covered by this residual glass compounds, then the contact resistance of the Ag/Si interface will be higher. It is essential to reduce the amount of this residual glass compounds by physical or chemical means. In this study, two different approaches are applied to reduce the contact resistance of the Ag/Si interface. The first one is to decrease the amount of glass residuals at the interface by using silver pastes with nano-sized non-glass frits. Owing to its high surface area, the resultant silver pastes possess excellent etching ability and therefore a shorter firing duration. Compared to silver pastes with conventional micro-sized glass frits, silver pastes with nano-sized non-glass frits produce very thin and discontinuous residual glass layer at the Ag/Si interface. The second method is to apply a silver coating on the surface of nano-sized additives via electroless plating method. With the silver coating, ceramic additives keep discrete during the firing step and this ensures the residual glass compounds are separated from each other. Hence a further improvement is obtained by applying the silver-coated non-glass ceramic additives in the screen-printable silver pastes [3].

1.3. Light-Emitting Diodes

Solid-state lighting (SSL) based on light emitting diodes (LEDs) has replaced traditional lamp-based systems in a number of lighting applications, such as traffic lights, signs and displays, and significant advances in terms of light extraction efficiency have been reported in

recent years for GaN-based LEDs. These advances in chip-level design include various improvements to reduce the effect of an issue called “efficiency droop”, including the incorporation of quantum wells with large overlap to suppress the charge separation, the use of wide double-heterostructure active regions to reduce Auger recombination issue, the reduction of polarization effect within the multiple-quantum well region to minimize the electron leakage, and new barrier designs to suppress the efficiency droop issue [4-6]. Packaging technologies and materials also hugely affect the light extraction efficiency and there are continuously advancements in LED packaging materials and technologies, including the addition of backside reflector, novel chip surface optical structures for light extraction and new packaging methods, which include multi-layered phosphor for white LEDs, new reflector cup materials, and new encapsulation materials with improved thermal and radiation resistance [7].

The largest market for light emitting diodes (LEDs) is liquid crystal display (LCD) backlighting unit (BLU) applications, although the highest growth rate now is the general lighting. Mid-power white LED emitters (30 to 150 mA input current) based on sapphire substrate with standard MESA structure are currently the dominant LEDs for LCD BLU applications, and they also appear to dominate general lighting applications because of their highest performance to cost ratio by offering designers and engineers a less expensive option in comparison with high-power LEDs and also better light output control, in terms of both brightness and light uniformity.

Extensive studies have been carried out on the role of die attach adhesives (DAAs) in the thermal behavior of packaged LED emitters, especially for high-power LEDs [8-10]. Die bonding materials include die attach adhesives, solder pastes, and eutectic alloys. Die attach

adhesives are the most common bonding materials for LED applications because the ease of application, and low cost of both materials and process [8, 10].

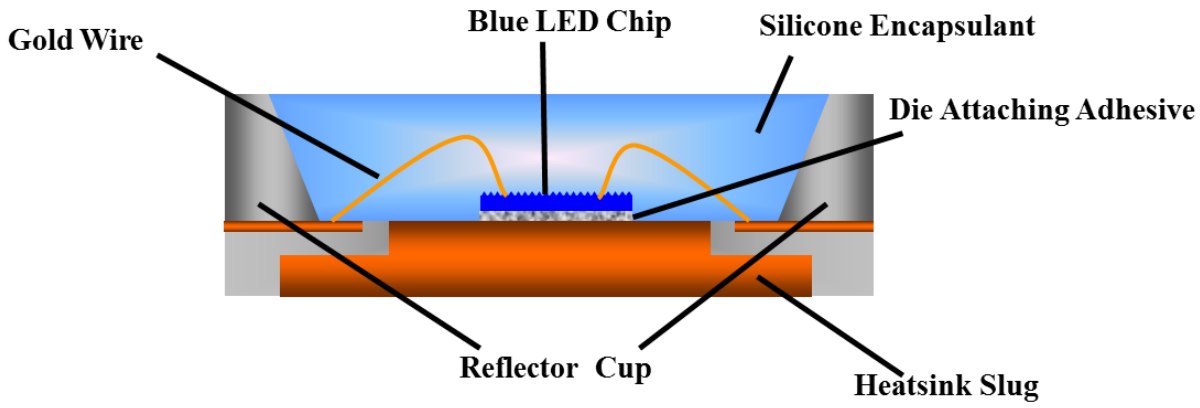

Fig. 1.3. The schematic drawing of the cross-sectional view of a monochromatic blue LED emitter with pure silicone encapsulant.

Figure 1.3 shows the schematic drawing of the cross-sectional view of a monochromatic blue LED package with pure silicone encapsulant [3]. The LED packaging components include a blue LED chip, die attach adhesive used to bond the chip onto the substrate, gold wires for connection of electrodes, silicone encapsulant (with phosphor for white LED packaging), and the leadframe, which consists of the reflector cup and the heatsink slug. Although the optical impact of the essential packaging materials, such as encapsulant and the reflector cup, is evident and has been well studied as well, no study has been reported on the optical performance of DAAs on either monotonic color LED or white LED emitters. This is probably because the extreme small amount (less than 10 mg) of DAAs used for attaching one LED die onto the substrate. Thus the

objective of the present work is to study the role of DAA materials, including optical clear, optical reflective and the conventional silver-based DAAs, in influencing the lumen output of both blue and white LEDs under different conditions, as well as the interaction between the chip and its components, and different DAA materials.

Important packaging parameters, such as bondline thickness and fillet coverage, are also crucial and important for the resultant light extraction efficiency. Fillet coverage is how much the side wall covered by the DAA materials. Figure 1.4 illustrates a blue LED chip with standard MESA structure and how the fillet covering the chip. It is important to obtain a fillet after die bonding process due to two reasons: first with a uniform fillet, it is ensured that there is no empty space between the chip and the substrate. The second reason is that when performing wire-bonding, a certain degree of shear vibration will be introduced. With a uniform fillet covering around the chip, it provides better mechanical support and prevents this chip from pull-up during wire-bonding. The effect of fillet coverage on LED light extraction efficiency is studied and the mechanism is elucidated.

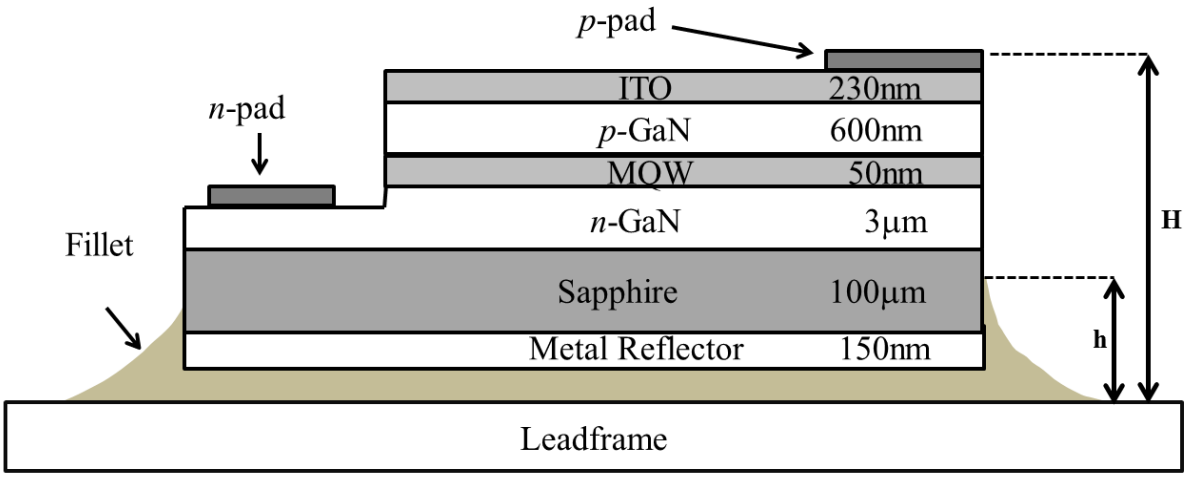

Fig. 1.4. The cross-sectional profile of a blue LED chip with standard MESA structure. The drawing is not in real ratio in order to distinguish and emphasize different layers.

Reference

[1]. R.R.A. Syms and J.R. Cozens, "Optical Guided Waves and Devices", McGraw-Hill (1992)

[2]. B.T. Dai and H.C. Chen, "Handbook of Solar Cells and Battery Technology", The Electronics and Materials Association (2008)

[3]. Y.C. Shih, Y.H. Lin, J.P. You and Frank G. Shi, "Screen-printable Silver Pastes with nano-sized Glass Frits for Silicon Solar Cells", *J. Electron. Mater.*, Vol. 42, No. 3, pp.410-pp. 416 (2013)

[4]. J. Piprek, "Efficiency droop in nitride-based light-emitting diodes", *Phys. Status. Solidi. A*, Vol. 207, No. 10, pp. 2217-2225 (2010)

[5]. N.F. Gardner, G.O. Muller, Y.C. Shen, G. Chen, S. Watanabe, W. Gotz and M.R. Krames, "Blue-emitting InGaN-GaN double-heterostructure light-emitting diodes reaching maximum quantum efficiency above 200 A/cm^{2}", *Appl. Phys. Lett.*, 91, 243506 (2007)

[6]. G. Liu, J. Zhang, C.K. Tan and N. Tansu, "Efficiency-Droop Suppression by Using Large-Bandgap AlGaInN Thin Barrier Layers in InGaN Quantum-Well Light-Emitting Diodes", *IEEE Photonic. Tech. L.*, vol. 5, No. 2, 2201011 (2013)

[7]. J.P. You, N.T. Tran, F.G. Shi, "Light extraction enhanced white light-emitting diodes with multi-layered phosphor configuration", *Opt. Express*, vol. 18, No. 5, pp. 5055-5060 (2010)

[8]. B. Yan, J.P. You, N.T. Tran, Y. He, F.G. Shi, "Influence of Die Attach Layer on Thermal Performance of High Power Light Emitting Diodes", *IEEE Trans. Compon. Packag. Manuf. Tech.*, vol. 33, No. 4, pp. 722-727 (2010)

[9]. Y.H. Lin, J.P. You, Y.C. Lin, N.T. Tran, F.G. Shi, "Development of high-performance optical silicone for the packaging of high-power LEDs", *IEEE Trans Compon. Packag. Manuf. Tech.*, vol. 33, No. 4, pp. 761-766 (2010)

[10]. V.R. Manikam and K.Y. Cheong, “Die Attach Materials for High Temperature Applications: A Review”, *IEEE Trans. Compon. Packag. Manuf. Tech.*, vol. 1, No. 4, pp. 457-478 (2011)

CHAPTER 2

SCREEN-PRINTABLE SILVER PASTES WITH NANOSIZED GLASS FRITS FOR SILICON SOLAR CELLS

2.1 Introduction

Screen printing is the technique commonly used to form the front-side contacts on silicon photovoltaic cells due to its cost- and time-effectiveness compared with other metallization techniques such as photolithography or light induced electroplating [1, 2]. Silver pastes primarily consist of three constituents: (1) metal silver powders with average particle size from 1 to 5 μm, which provide the conductive phase in the resulted films due to its superior conductivity, high chemical stability and lower price among the noble metals; (2) glass frits and oxide additives, which enable and enhance the binding of the silver phase to the silicon substrates; and (3) organic phases, which disperse the metal and binder components to impart the desired rheological properties to the pastes [3].

The formation of silver front-side contacts via screen-printing includes three major steps: firstly the silver paste is screen-printed on the surface of silicon wafers to form the electrode lines. The second step is to dry the wafers at around 180-220^{o}C so the solvent in the silver paste can be evaporated. The wafers will then go through a firing process at around the Ag-Si eutectic temperature (835^{o}C) to burn out the organic phase and make the silver electrodes denser. Figure 2.1 shows the Ag-Si phase diagram and the eutectic point of 835^{o}C [4].

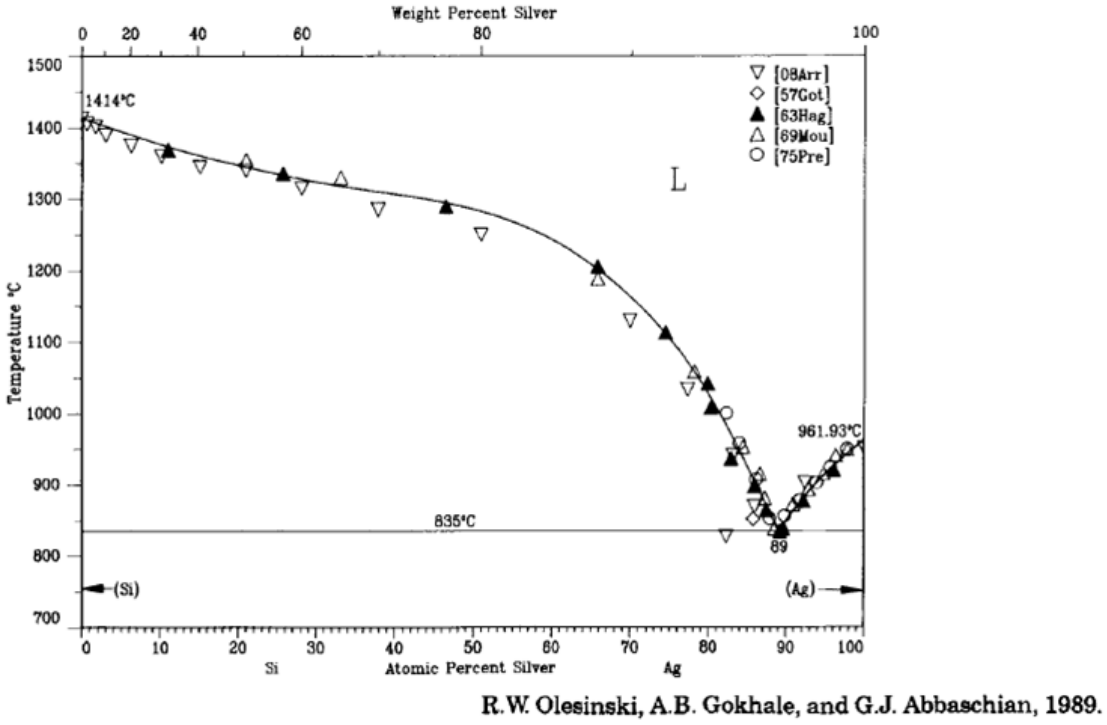

Fig. 2.1. Ag-Si system

During the firing process the paste will etch through the anti-reflect coating (ARC) layer and form the Ag-Si eutectic structure at the interface of Ag/Si layers and this structure will act as a conductive channel which allows the electrons to flow through [1]. Therefore the interface formed after the heat treatment plays the most important role regarding the conductivity.

Glass frits and oxide additives, despite holding the minimum weight percentage, usually < 10%, are very essential compositions in the silver pastes. During the firing process glass frits and oxide additives can help etch through the ARC layer and establish stable mechanical and electrical conductive contacts between silver contacts and the silicon layers [1, 5]. The residual glass, however, will accumulate at the surface of silicon wafers and form insulating layers between silver electrodes and silicon layers [1, 5-8]. The thickness and properties of the post-

firing insulating layers are the determining factors for the electrical properties and performance in the solar cells. In order to maximize the conductivity of the solar cell system, the thickness of the residual glass layer must be minimized and a long proportion of Ag/Si eutectic structure must be established at the interface.

It is important and essential to choose the correct glass components in order to meet the desired electrical and mechanical properties for the silver paste and the firing process. The softening point of a usable glass binder must be around 450-550^{o}C so that the silver paste could be sintered at around the Ag/Si eutectic temperature which is 835^{o}C. If the softening point is lower than 450^{o}C, the sintering is advanced and then the desired conducting channel would not be achieved. If the softening point is higher than 550^{o}C, the sufficient adhesive strength will not be exerted because a sufficient melting flow is not caused during the firing process [9]. Some components in glass frits, such as Pb, Bi and Al, can also aid the formation of silver crystalline precipitated in the residual glass/silicon interface and therefore lead to further improvement on electrical performance [3, 6, 7]. Although lead is excellent component for both mechanical and electrical properties, the use of lead is prohibited because it is highly toxic and the production of lead content pastes is potentially hazardous [3, 6]. Bismuth is found to be a good substitute to fabricate the lead-free products [1, 3]. Numerous oxide additives were tested and zinc oxide was found to be the top performer by effectively diminishing the residual glass layers [8].

There are many factors which can affect the electrical performance of silver pastes. In this work we will focus on the size effect of the glass frits upon the resulted microstructures at the Ag/Si interfaces, and with different interfacial microstructures it will subsequently lead to different electrical performances. The size effect of silver particles in the metallization pastes had been investigated and the results showed that pastes with small (several micrometers) and

spherical silver particles gave the best electrical performance [10]. There are many glass frits and oxide additives which had been well studied and compared, but in order to avoid the complex interactions among these components, only Bi_2O_3, SiO_2, Al_2O_3 and ZnO were chosen to be used in this study due to their excellent performance for the enhancements of electrical and mechanical properties [2, 8, 11]. Different formulae with micro- and nano-sized glass frits were compared and the optimal formulae for glass frits with different sizes were found along with the firing conditions. Advanced microscopy techniques such as scanning electron microscopy (SEM) equipped with an energy-dispersive X-ray spectrometer (EDX), and focus ion beam (FIB) technique were carried out in order to investigate the Ag/Si interfaces and the results were compared with the electrical performance acquired by transfer length method (TLM) [12]. Transfer length method is a technique used to measure the specific contact resistivity between two layers. The procedure is simple with a probe station, which is illustrated in Fig. 2.2.

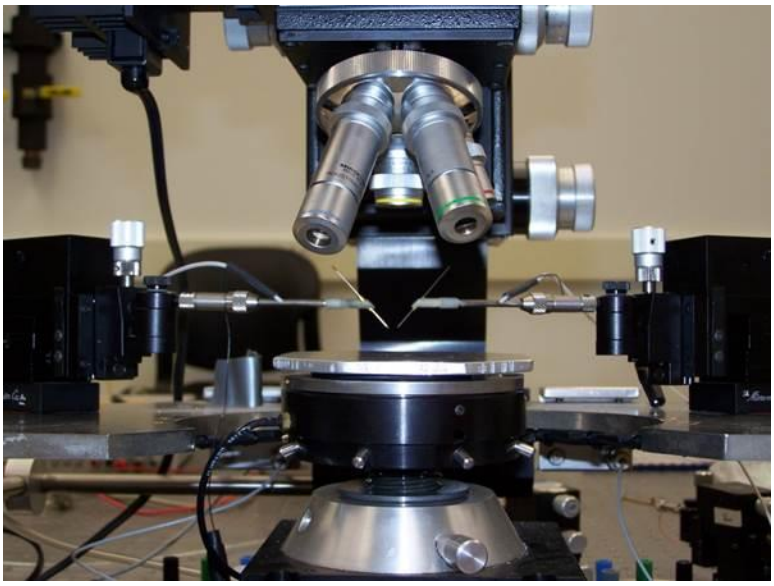

Fig. 2.2. The probe station for electrical measurement.

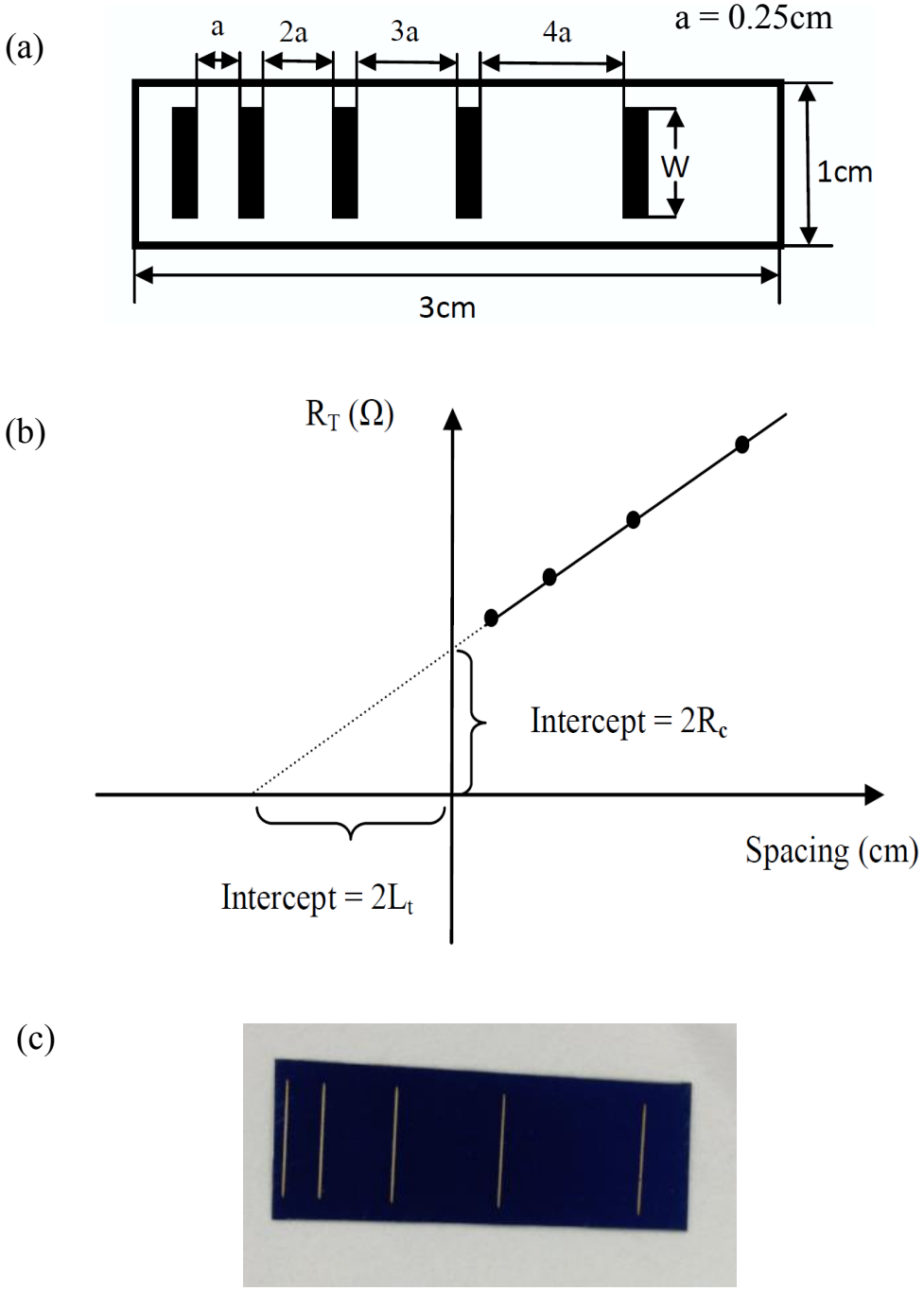

Figure 2.3. (a) Schematics of the TLM patterns used in this work with a=0.25 cm, (b) a generic TLM result for determining the specific contact resistivity and (c) the image of an actual sample in this work.

Figure 2.3 is the schematics of the TLM patterns used in this study and a generic TLM result for determining the specific contact resistivity. The specific contact resistivity (ρ_c) is obtained from extrapolating this linear plot of total resistance (R_T) versus the pattern grid spacing (d) [11]:

$$\rho_c = R_c L_t W \tag{2.1}$$

here W is the length of the TLM patterns, as shown in Fig. 2.3(a).

2.2 Experimental

In this work ceramic components with different sizes are commercial available from Alfa Aesar and were used to form the glass frits. Table 2.1 summarized the particle sizes of the glass frits and the micro- and nano-sized frits were denoted as glass A and B, respectively. The micro-sized ceramic components were milled to an average size of 1μm prior to use. The following procedure was used for the preparation of silver pastes: first the appropriate amounts of solvent, polymer medium and surfactant were well mixed and aged at 40^{o}C for 24 hours. Silver powder, with an average size of 2μm, was mixed with above-discussed organic medium and glass frits in a Thinky (Thinky USA) mixer for four minutes and followed by a de-airing for 10 seconds. In order to ensure better mixing and to avoid the agglomeration, the solid phase was added into the organic medium incrementally. Table 2.2 shows the compositions of the different formulae used in this experiment.

Table 2.1 Average particle size of ceramic components employed in this study.

	Bi_2O_3	Al_2O_3	SiO_2	ZnO
Glass A	2 µm	1.5 µm	2 µm	2.5 µm
Glass B	140 nm	45 nm	80 nm	70 nm

Table 2.2 Silver compositions (wt%) of the silver pastes.

Sample Code	Glass	Glass frits				Total Ceramics	Silver	Organic Medium
		Bi_2O_3	Al_2O_3	SiO_2	ZnO			
GA-1	A	4.24	2.13	2.95	2.10	11.42	68.58	20
GA-2	A	2.12	1.07	1.00	1.10	5.29	74.61	20
GB-1	B	1.28	0.23	0.48	3.00	4.99	69.01	26
GB-2	B	0.66	0.13	0.25	2.10	3.14	71.86	25

The pastes were then screen-printed on 3 cm x 1 cm and 200 µm thick *n*-type (100) Cz Si wafers with an 80 nm thick SiN_x ARC layer above. Three samples were made for each silver paste by the same procedure. The screen-printed wafers were then dried at 180^{o}C for 15 minutes. During this step the solvent in the Ag electrodes was evaporated and the color of the electrodes changed from brown to white. After the drying process, the wafers were fired and sintered at 880^{o}C. The sintered wafers were tested by Agilent 4156A under dark condition to get the total resistance and the results were plotted according the TLM illustration shown in Fig. 2.3(b) to

determine the specific contact resistivity for these samples. According to the TLM results, the optimal firing time for each paste was found and compared. Samples made with different firing conditions were also investigated in order to clarify the influence of heat treatment on the microstructure and electrical performance.

Advanced microscopy techniques were employed in order to examine the difference in electrical performance caused by the interfacial microstructure. Scanning electron microscopy (Philips XL-30 FEG) observations with EDX and FIB/SEM (FEI 5 Quanta 3D FEG) technique were employed in this study to investigate the interfacial microstructures between the front-side electrodes and the silicon wafers. The observations were carried out in backscattered electron mode in order to show the difference between silver and glass phases more apparently.

2.3 Result and Discussion

In the following discussion, four different groups of samples made by glass frits A and B will be denoted as GA-1, GA-2, GB-1 and GB-4, respectively. Table 2.3 shows the TLM results and the firing conditions for the silver pastes employed in this study. According to Table 3, GB-1 shows the best electrical performance and also the shortest firing duration among all the tested samples. Based on this table we could compare the results based on the following groups.

Table 2.3 TLM results for tested samples with various firing conditions.

Sample code	Total glass and oxide wt.%	Firing conditions	ρ_c (Ωcm^2)				Average R_c (Ω)
			Sample 1	Sample 2	Sample 3	Average	
GA-1	11.42	60s/880 °C	0.1408	0.1441	0.1411	0.1420	22.19
GA-2	5.76	300s/880 °C	0.0372	0.0362	0.0364	0.0366	5.72
GB-1	4.99	20s/880 °C	0.0123	0.0157	0.0152	0.0144	2.25
GB-2	3.14	50s/880 °C	0.0231	0.0233	0.0220	0.0228	3.56
GB-1-30	4.99	30s/880 °C	0.0330	0.0312	0.0321	0.0321	5.02
GB-1-40	4.99	40s/880 °C	0.0257	0.0255	0.0268	0.0260	4.06
GB-1-960	4.99	20s/960 °C	0.0177	0.0169	0.0176	0.0174	2.72

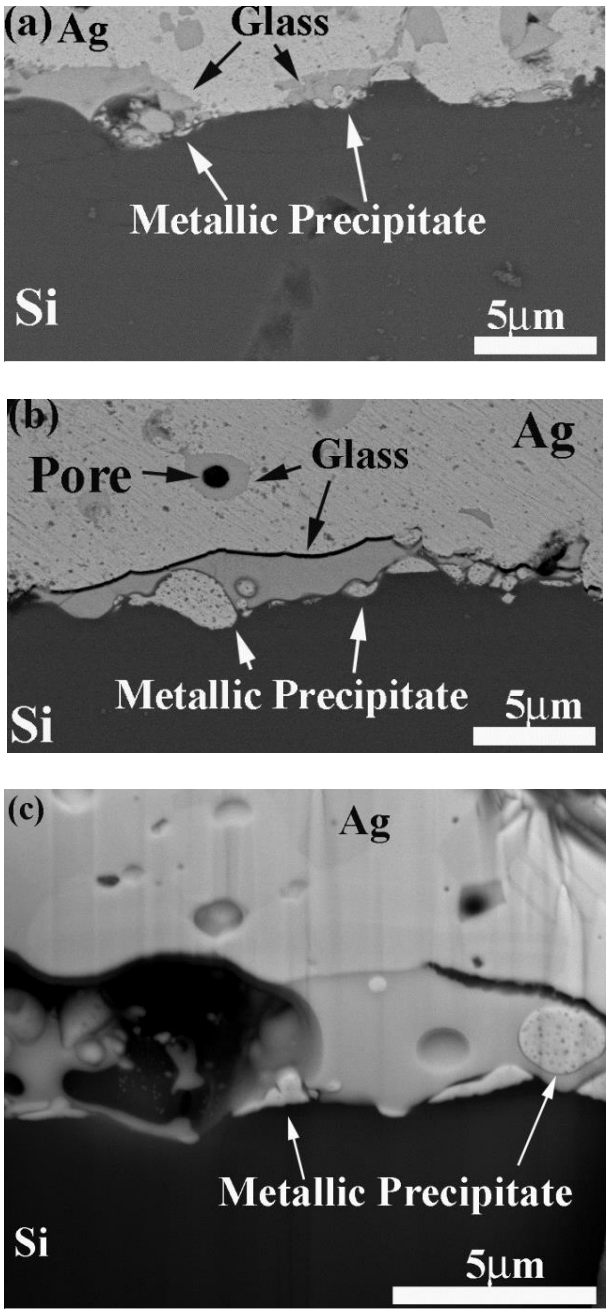

Figure 2.4. SEM BSE images of tested samples made by glass frits A: (a) GA-1, (b) GA-2 and (c) the FIB images of GA-2

2.3.1 Comparison between GA-1 and GA-2

GA-1 and GA-2 used the same glass frits but in different weight percentage. It is reasonable that with less etching agents it should take longer time for GA-2 to achieve optimal performance because the etching rate is lower. Figure 2.4 is the microstructure obtained by SEM for GA-1 and GA-2. In Figure 2.4(a) and (b) it shows that there are residual glass layers between Ag and Si, and there are also some metallic precipitates formed between the glass and Si layer. The Ag/Si eutectoids and metal alloy precipitates, mostly were silver and bismuth, were initially formed in the glass/Si interface and then grew backward to the Ag/glass interface. The silver and bismuth ions, dissolved in the softened and fluidized glass, were brought to the interface and form the eutectoids and metal precipitates on the surface of silicon layers [1]. If the precipitates grew big enough, the conductive channel between Ag bulk and the silicon layer could be built. From the SEM images there was less residual glass at the Ag/Si interface in GA-1 because of the shorter firing duration, and even it contained more glass frits initially. However due to the shorter firing duration, the metallic precipitates were smaller than those in GA-2, as seen in Figure 2.4(b), and therefore the resistivity of GA-1 is much higher than GA-2 since there were only few conducting channels formed within the residual interfacial glass layer. In GA-2 the metallic cluster had grown large enough to form the conducting channels despite the thick glass layer. This implies the reason why it required such a long firing duration for this formula to achieve the optimal electrical performance. Figure 2.4(c) is the FIB/SEM image of GA-2 and it also shows the pores and metallic precipitates in the microstructure. The circular pores in the FIB/SEM image were the evidences of nitrogen trapped inside the glass layer after the firing process. While cooling down, the nitrogen and the glass frits formed an amorphous layer

between Ag bulk and Si. If the composition was far from stoichiometry, a nitrogen bubble would form [8].

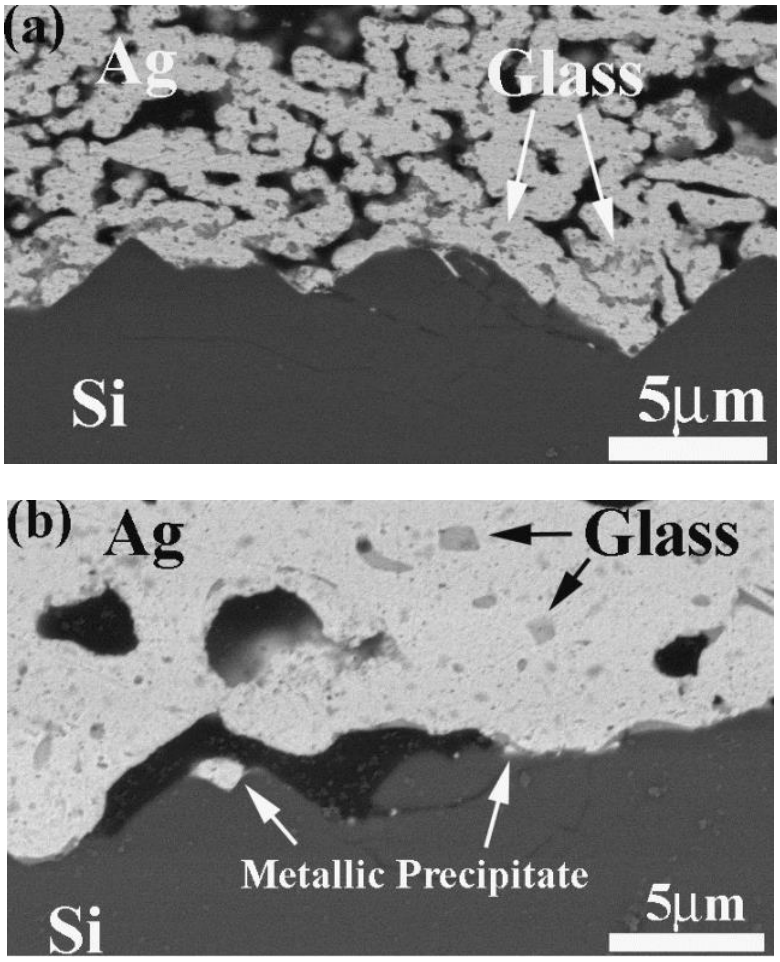

Fig. 2.5. SEM BSE images of tested samples made by glass frits B: (a) GB-1 and (b) GB-2

2.3.2 Comparison between GA-2 and GB-1

From the TLM results, the specific contact resistivity of GB-1 is better than that of GA-2 and the firing duration is much less. Figure 2.5(a) shows the microstructure of GB-1. The porous Ag bulk is a result of short firing duration and more organic medium in this paste. The extra organic medium in this formula was because the nano-sized glass frits possessed higher surface area in this formula. It is noticeable that there is only a little interfacial glass remaining in the Ag/Si interface. Because the residual glass is not continuous at the interface, the Ag layer could form conducting channels directly with Si layer without relying on the formation of the metallic precipitates mentioned above. The best ρ_c obtained in this work is 0.0123 Ωcm^2 as listed in Table 2.3 for the first sample of GB-1. This value is close or even better than results from other research which applied similar glass frits systems [1, 2]. Because the best value obtained by Cho etc. [1] was under a special firing condition with pure oxygen ambient, the method proposed in this work to achieve better contact might be more applicable for real applications.

The SEM results show that the nano-sized glass frits has better etching ability and therefore the required firing duration is shorter, which can prevent the residual glass from accumulating at the Ag/Si interface. This enabled the formation of the Ag/Si eutectic structures in a large scale. Although the Ag bulk is more porous in GB-1, the overall conductivity is still better because there is less glass residue near the Ag/Si interface, which leads to a better interfacial property for the purpose of electrical conductivity. The better interfacial property will ensure better electrical performance and this corresponds to the results from the TLM measurements. This porous structure could also behave as escape channels for nitrogen and burned organic medium during the firing process and therefore the residue of glass frits was

further diminished. Even glass frits B consisted of less silver content, the porous but continuous Ag bulk was still more conductive than the Si-layer. From the images it shows that the residual glass was dispersed uniformly in the Ag bulk after the firing process. This is because the ceramic compositions did not have enough time to flow and diffuse to the surface of Si-layer due to the shorter firing duration. Even both formulae consisted of almost the same amount of ceramic compositions, most ceramic compositions in GB-1 dispersed uniformly in the Ag bulk but in GA-2 they will accumulate at the interface due to the long firing duration.

For GA-2 although the Ag bulk is denser due to the long firing duration, the specific contact resistivity is still higher. The firing duration was much longer than that of GB-1 and with increased firing time, the energy consumption and cost will also increase while the producing rate will decrease. Therefore if we examine and compare the two pastes used in this study, the paste made by nano-sized glass frits is more cost-effective and productive in the aspects of firing duration and electrical performances.

2.3.3 Comparison between GB-1 and GB-2

GB-2 was used to see if the amount of glass frits could be further reduced. The optimal firing duration increased as expected but the electrical performance was worse than that of GB-1. From the microstructure shown in Figure 2.5(b), this result could be explained. In Figure 2.5(b) there is a continuous thin glass layer at the interface and this is the reason the specific contact resistivity is higher. Although there were some metallic precipitates formed at the interface, they were too small to become useful conducting channels due to the lack of ion carriers resulted from

less glass frits. Based on this the proper amount of glass frits is required in order to achieve the best interface properties.

2.3.4 Influence of firing conditions on the interface microstructure

Figure 2.6 shows the interface microstructures of samples made by GB-1 with different firing conditions and the TLM results of these samples are listed in Table 2.3. From Fig. 2.6 (a) and (b) it shows that the Ag bulk becomes denser as the firing duration increases. The glass components were trapped in the Ag bulk regime and accumulated together to form bigger clusters as the firing time increased. The TLM results indicate that GB-1-40 possesses a lower ρ_c. From the SEM observation this might be resulted from the longer firing time which led to larger Ag precipitates at the glass/Si interface. Figure 2.6 (c) shows the interface microstructure of samples fired at 960 ^{o}C and it also shows a denser Ag bulk in comparison with GB-1. Because the firing time was short, small glass clusters were uniformly dispersed in the Ag bulk regime. ρ_c of GB-1-960 is only slightly higher than that of GB-1 and this might be due to the short firing duration. Although the glass clusters were larger with higher firing temperature, the remaining glass frits did not have enough time to diffuse to the Ag/Si interface and form a continuous insulting layer there. Based on TLM results and SEM observation, firing duration could hugely affect the microstructure at the Ag/Si interfaces and the value of ρ_c, while rising firing temperature will cause obvious effect on the microstructure but only slightly increases the electrical performance.

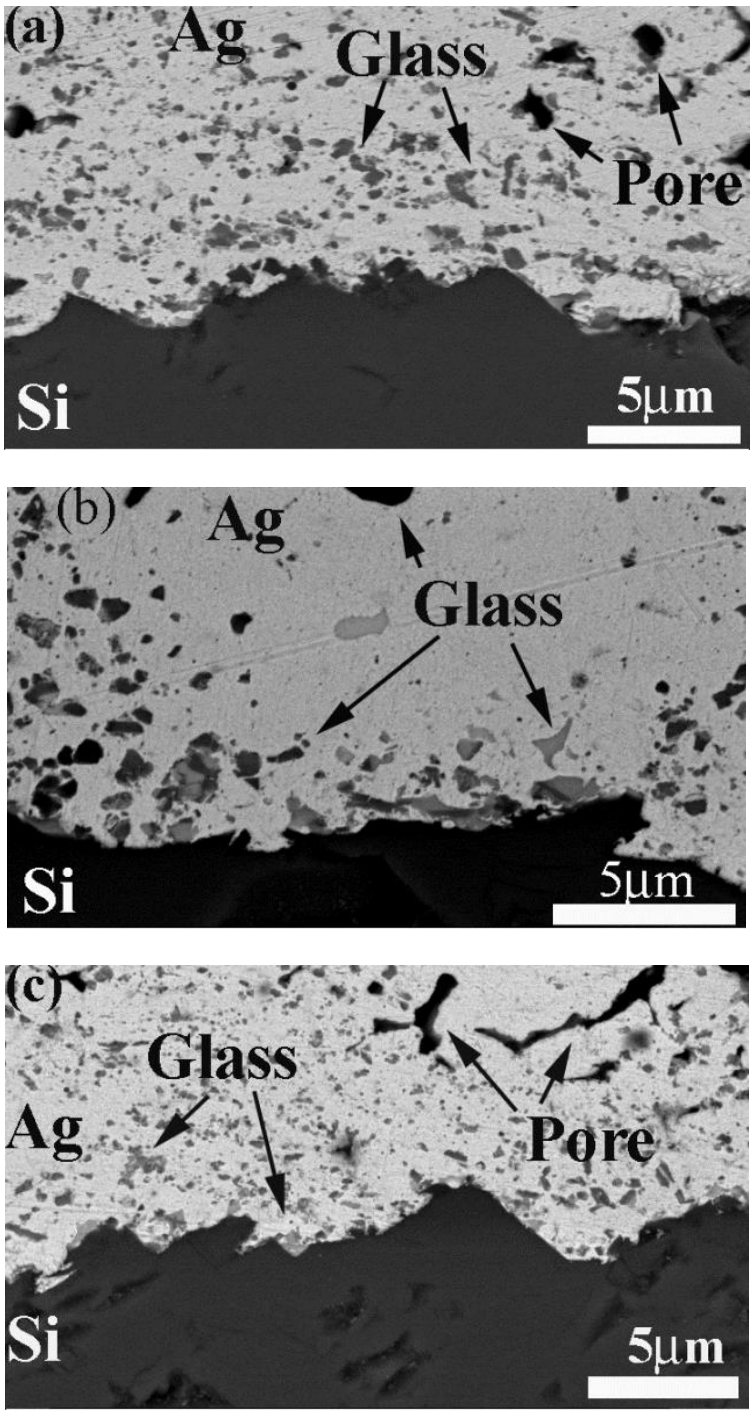

Fig. 2.6. SEM BSE images of tested samples made by silver paste GB-1 with different firing conditions: (a) GB-1-30 (b) GB-1-40 and (c) GB-1-960.

2.4 Conclusion

The size effect of glass frits and oxide additives was examined in terms of electrical performances and microstructures of samples made by silver pastes consisting of different sized glass frits. The microstructures and TLM results are corresponding to each other and indicated that the silver paste with nano-sized glass frits made better electrical contacts at the Ag/Si interfaces. The specific contact resistivity of a metallization contact is strongly affected by the interfacial microstructure and firing duration. Silver pastes with nano-sized glass frits were proven to be more efficient for the purpose of etching though the ARC layer. Due to the high efficiency it could also prevent ceramic compositions from accumulating at the interface by shortening the duration of thermal treatment and therefore the Ag/Si eutectic structures could be formed at the interface in a very large and continuous proportion. The results in the samples made by micro-sized glass showed that the metallic precipitates formation at the glass/Si interface was attributed to the reaction between the silver ions dissolved in the softened glass compositions and silicon ions. This implied the necessity of a long thermal treatment for this formula.

Low resistivity is the most desirable property for the silver metallization contacts used in solar cells. Nano-sized glass frits could provide better, more uniform and complete etching of the ARC layer, which resulted in a lower specific contact resistivity for the crystalline silicon photovoltaic cells. The use of nano-sized glass frits versus micro-sized glass frits in silver metallization pastes was found to be more beneficial in terms of better electrical performances, shorter processing durations, lower cost and energy consumption. The results from this present study demonstrate that the particle size of ceramic compositions in silver pastes could be a very

important parameter to be carefully controlled in order to achieve the desirable quality of ohmic contacts for crystalline silicon photovoltaic cells.

References

[1]. S.B. Cho, K.K. Hong, B.M. Chung, and J.Y. Huh, *Proceedings of the 34th IEEE Photovoltaic Specialists Conference* (New York: IEEE, 2009), pp. 766-769.

[2]. Y. Zhang, Y. Yang, J. Zheng, G. Chen, C. Chen, J.C.M. Hwang, B.S. Ooi, A. Kovalskiy, and H. Jain, *Thin Solid Films* 518, 111(2010).

[3]. S.B. Rane, T. Seth, G.J. Phatak, D.P. Amalnerkar, *J. Mater. Sci.: Mater. Electron*. 15 103 (2004).

[4]. R.W. Olesinski, A.B. Gokhale and G.J. Abbaschian, "The Ag-Si (Silver-Silicon) System", *Bulletin of Alloy Phase Diagrams*, Vol. 10, No. 6. Pp. 635-640 (1989).

[5]. M.M. Hilali, S. Sridharan, C. Khadilkar, A. Shaikh, A. Rohatgi, and S. Kim, *J. Electron. Mater.*, vol. 35, No. 11, pp. 2041 (2006).

[6]. S.B Cho, K.K. Hong, J.Y. Huh, H.J. Park, and J.W. Jeong, *Curr. Appl. Phys*. 10, 222 (2010).

[7]. K.K. Hong, S.B. Cho, J.S. You, J.W. Jeong, S.M. Bea, and J.Y. Huh, *Sol. Energ. Mat. Sol. C*. 93, 898 (2009).

[8]. A.S. Ionkin, B.M. Fish, Z.R. Li, M. Lewittes, P.D. Soper, J.G. Pepin, and A.F. Carroll, *ACS Appl. Mat. Interfaces* 3, 606 (2011).

[9]. Takuya Knno, Takashi Kitagaki, and Hiroki Kojo, US patent No. 7,767,254 B2.

[10]. M.M. Hilali, K. Nakayashiki, C. Khadilkar, R.C. Reedy, A. Rohatgi, A. Shaikh, S. Kim and S. Sridharan, *J. The Electrochem. Soc*. 153, 5 (2006).

[11]. Alan Frederick Carroll and Keneth Warren Hang, US patent No. 7,935,277 B2.

[12]. Dieter K. Schroder, *Semiconductor Material and Device Characterization, 2nd ed.* (New York: John Wiley & Sons, 1998), p. 156.

CHAPTER 3

NOVEL NON-GLASS FRITS FOR SCREEN-PRINTABLE SILICON SOLAR CELL METALLIZATION

3.1 Introduction

Nano-sized ceramic additives have been proved to effectively reduce the thickness of the discontinuous residual glass layer due to their excellent etching ability, and specific contact resistance between Ag/Si interfaces of samples made with nano-sized ceramic additives is only about 40% of that of samples made with micron-sized ones [1-4]. Ceramic additives with smaller size possess larger surface area and therefore can achieve faster etching rate to remove the Si_3N_4 anti-reflection layer (ARC) layer with less amount, which also reduce the firing duration and therefore prevent the residual glass from accumulation at the Ag/Si interface. The silver electrodes remain porous after the firing process and thus provide an escaping route for nitrogen produced from the firing process. If the nitrogen cannot escape from the interface, it will either form a bubble, or react with the residual ceramic components and form the glass layer, and either result will introduce extra resistance to the Ag/Si interface. Therefore the use of nano-sized ceramic additives is beneficial in terms of electrical conductivity, which enhances the overall efficiency of the solar photovoltaic, and process duration, which reduces the cost and increases the production rate.

In this work, in order to further reduce the contact resistance at the Ag/Si interface, nano-sized ceramic additives with silver coating by electroless plating method were employed to form the silver paste. Silver coating on the ceramic additives can prevent them from directly contacting with each other during and after the firing step. Even a phase separation between silver coating and ceramic substrates happens during the firing steps, these two materials remain close to each other if the firing duration is very short. Electroless plating technique has attracted much attention in the semiconductor industries due to its low processing temperature, low overall cost, high coverage and uniform coating [5-7]. Moreover, electroless plating can deposit metals onto substrates with complex shape and the process does not require a vacuum system. Coating coverage and thickness can be easily controlled by changing the processing parameters, such as activation time, plating duration, and pH value. Electroless silver plating has been well developed and applied to deposition of metallic silver onto various substrates, such as micron-sized spheres and rods, nanoparticles and glass substrate for microcontact [5-7]. Different formulae were employed to investigate the effect of silver plating on the etching rate and the resultant specific contact resistance. To avoid the complex interaction between different ceramic components at high firing temperature, only Bi_2O_3, Al_2O_3, fused SiO_2 and ZnO were used in this work, and the firing condition including firing temperature and duration is same as our previous study [3]. In order to main the function of ceramic additives, parameters of electroless plating were controlled to obtain a partially coverage of silver coating on the ceramic substrates. Transmission electron microscopy (TEM) and X-ray diffraction (XRD) were used to identify the silver deposition on the ceramic additives. Scanning electron microscopy (SEM) was applied to investigate the Ag/Si interface, and the results were compared with the electrical performance acquired by the transfer length method (TLM).

3.2 Experimental

In this work all four nano-sized ceramic components are commercial available from Alfa Aesar. Table 3.1 summarizes the composition of different silver paste formulae used in this work. The following procedure was used for the preparation of silver pastes: first the appropriate amounts of solvent and polymer medium were well mixed and aged at 40^{o}C for 24 hours. Silver powder, with an average size of 2 µm, was mixed with above-discussed organic medium and ceramic additives in a Thinky (Thinky USA) mixer for four minutes and followed by a de-airing for 10 seconds. In order to ensure better mixing and to avoid the agglomeration, the solid phase was added into the organic medium incrementally.

Table 3.1. Composition (wt.%) of silver pastes for different samples

Sample Code	Ceramic Additives				Total Ceramics	Silver	Organic Medium
	Bi_2O_3 (140nm)**	Al_2O_3 (45nm)**	SiO_2 (80nm)**	ZnO (70nm)**			
N-1	1.28	0.23	0.48	3.00	4.99	75.01	20
NE-1	1.28	0.23*	0.48*	3.00	4.99	75.01	20
NE-2	1.28*	0.23*	0.48*	3.00*	4.99	75.01	20

*with electroless silver plating
**average particle size

$AgNO_3$ (99.95%) was obtained from Salt Lake Metals. Ethylenediamine and 3,5-diiodotyrosine were obtained from Sigma-Aldrich. Rochelle salt (potassium sodium tartrate) was obtained from Mallinckrodt Chemicals. Hydrochloric acid (36%) and nitric acid was obtained

from J.T. Baker. Stannous chloride dehydrate ($SnCl_2 \bullet 2H_2O$) was obtained from Alfa Aesar. All of these chemicals were used as received. The following procedure was used to form the electroless plating solution. First, the silver ion solution (denoted as solution A) and reducing agent solution (denoted as solution B) were prepared separately. Solution A is an aqueous solution composing of $AgNO_3$ and ethylenediamine. Solution B is composed of Rochelle salt and 3,5-diiodotyrosine in another aqueous solution. The two solutions were well-mixed to form the electroless plating solution right before the silver plating step. The activation solution is composed of stannous chloride dehydrate and hydrochloric acid.

The procedure is as follow: first the ceramic additives were poured into the activation solution to form the seed layer on the particle surface. Once the activation duration finished, the colloid was washed by isopropyl alcohol (IPA) twice and then centrifuged at 3000 rpm for 15 minutes. Once the supernatant was removed, water was added to form an aqueous solution for the next step. Solution A and B, as described above, were then mixed and the solution with ceramic additives was poured into this mixture for silver plating. During the plating, the pH value was controlled to be between 10.0 and 10.9 by diluted nitric acid. After the plating was ended, the same washing and centrifuging were performed twice. After removing the supernatant, IPA was added to form a solution. This solution was then placed in an oven at 85℃ to remove the solvent. Table 3.2 summarizes experimental parameters in the electroless plating step. The resultant powder was used to form the silver pastes described above.

Table 3.2. Composition and process conditions of activation and plating solutions for electroless silver plating

Activation Solution		Plating Bath	
Compound	Parameter	Compound	Parameter
$SnCl_2$·2H2O	$2.1x10^{-1}$ M	$AgNO_3$	$3.0x10^{-3}$ M
HCL (36%)	$3.4x10^{-1}$ M	Ethylenediamine	$1.8x10^{-2}$ M
		Rochelle Salt	$3.5x10^{-2}$ M
		3,5-diiodotyrosine	$4.0x10^{-5}$ M
pH	9.5-10.2	pH	10.0-10.9
Temperature	50℃	Temperature	50℃
Bathing Time	45 minutes	Bathing Time	3-10 minutes

The pastes were then screen-printed on 3cm x 1cm and 200μm thick *n*-type (100) Cz Si wafers with an 80nm thick SiN_x ARC layer on the top. TLM measurements were used to determine the specific contact resistivity under dark conditions. The pattern for TLM measurements is shown in Fig. 2.3 (a). Figure 2.3 (b) is the illustration showing the plotted TLM results for determining the specific contact resistivity of Ag electrodes. The specific contact resistivity (ρ_c) is obtained from extrapolating this linear plot of total resistance (R_T) versus the pattern grid spacing (d) [8]:

$$\rho_c = R_c L_t W \tag{2.1}$$

where R_c is the contact resistance, L_t is the transfer length and W is the grid length.

The screen-printed wafers were then dried at 180^{o}C for 15 minutes and then fired and sintered at 880^{o}C. The sintered wafers were tested by Agilent 4156A to get the total resistance and the results were plotted according the TLM illustration shown above to determine the

specific contact resistivity for these samples. Firing conditions and TLM results for different samples are summarized in Table 3.3.

Transmission electron microscope (FEI/Philips CM-20 conventional TEM) and X-ray diffraction (Rigaku SmartLab X-ray Diffractometer) were used to identify the silver coating on ceramic additives. Scanning electron microscope (Philips XL-30 FEG SEM) was used to investigate the microstructure at Ag/Si interfaces.

Table 3.3. TLM results of tested samples

Sample code	Total glass and oxide wt.%	Firing conditions	Average ρ_c (Ωcm^2)	Average R_c (Ω)
N-1	4.99	20s/880 ^oC	0.0144	2.19
NE-1	4.99	20s/880 ^oC	0.0109	1.70
NE-2	4.99	40s/880 ^oC	0.0221	3.45

3.3 Result and Discussion

Figure 3.1 shows TEM images of SiO_2 nanoparticle before and after electroless silver plating with plating time of 10 minutes. In Fig. 3.1 (b) there are small dots on the surface of SiO_2 substrates. Figure 3.2 shows the comparison of XRD patterns between pure SiO_2 and SiO_2 powder after 30-minute electroless silver plating. The plating time is prolonged to enhance the signal of silver plating. From the XRD patterns, SiO_2 after plating shows signals of metallic silver. The peaks of AgCl indicating that there are residual chloride ions after the activation step. With TEM images and XRD patterns, silver coating on the surface of ceramic additives is confirmed.

TLM results are summarized in Table 3.3. Sample N-1 consists of pure ceramic additives without any silver plating and this sample shows intermediate specific contact resistance among all different samples. For sample NE-2 with all four ceramic additives coated, because the silver coating actually blocks the contact between the etching agents (Bi_2O_3 and ZnO) and the Si_3N_4 ARC layer, etching rate of this paste is lowered and it takes long time to remove the ARC layer and form the conducting channel at Ag/Si interfaces. Sample NE-1 shows the lowest specific contact resistance among all three types of samples and is about 20% lower than N-1 in specific contact resistivity. Al_2O_3 and SiO_2 can enhance the adhesion between Ag electrodes and *n*-type silicon layers but they are not the major etching agents [3]. Therefore silver coating on the surface of these two additives does not affect the etching rate through ARC layers.

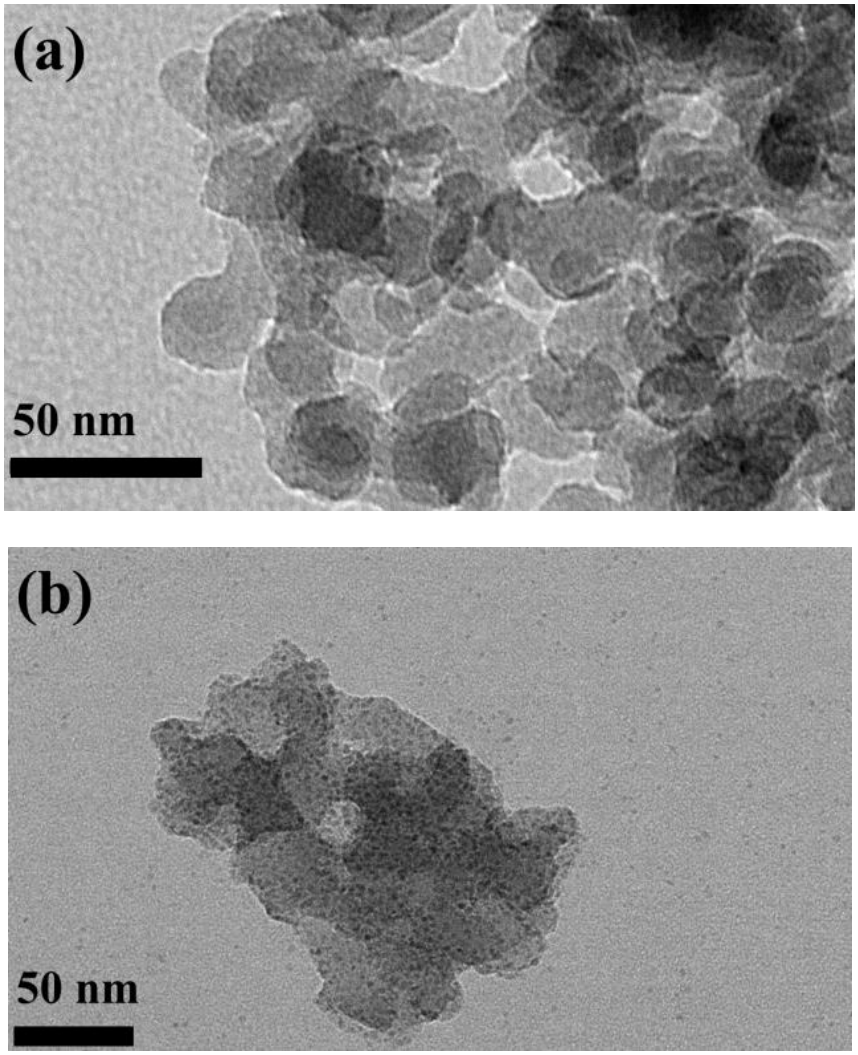

Fig. 3.1. TEM images of SiO_2 nanoparticles used in this work: (a) pure SiO_2 and (b) SiO_2 nanoparticles with silver coating and 10-minute plating time

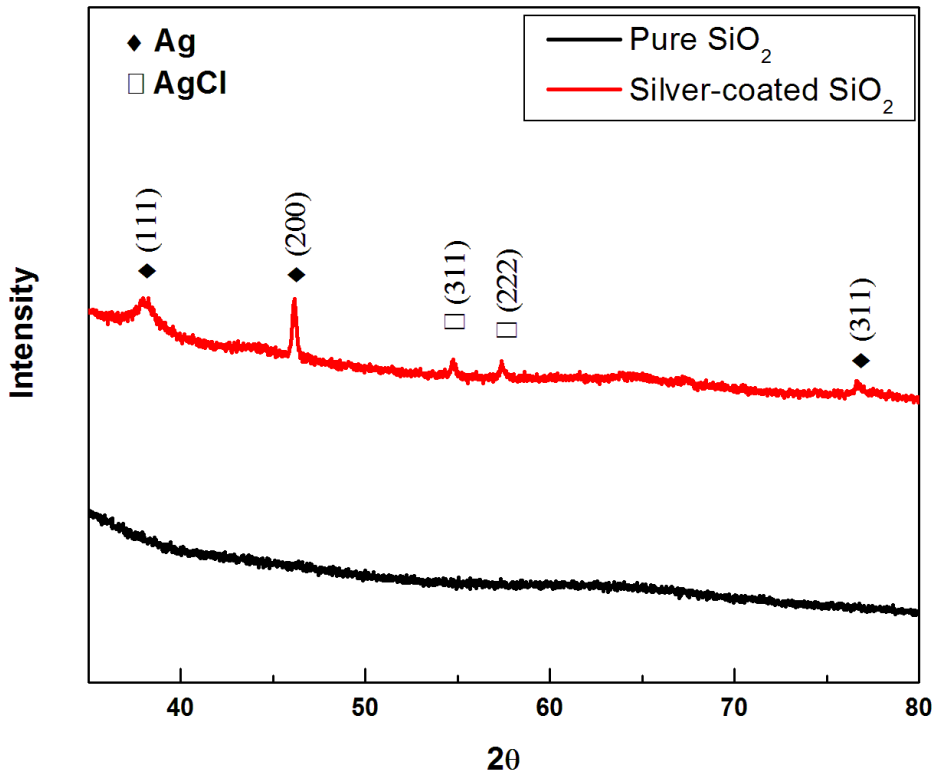

Fig. 3.2. XRD patterns of pure SiO_2 nanoparticles and silver-coated SiO_2 nanoparticles with 30-minute plating time

Bi_2O_3 and ZnO in NE-1 remain untreated so they also remain the same etching ability. Figure 3.3 shows SEM images for three different types of samples. For Fig. 3.3 (a) and (b), the images look very similar but the glass clusters in Fig. 3.3 (a) is larger. The difference in the size of residual glass clusters indicates that silver coating on the surface of ceramic compositions can ensure the formation of discontinuous residual glass clusters, as well as a discontinuous glass layer at the Ag/Si interface. The silver coating acts as a blocker between two nearby ceramic additives during the process and therefore adjacent ceramics do not touch each other during the entire process. Due to short firing duration, the pores and the large glass clusters near the interface can block the entire conducting route in the local section. Figure 3.3 (c) shows a denser silver electrode because the prolonged firing duration, which gives longer time for the residual glass to accumulate at the interface and cover most of the interface. However because the silver electrode is denser and all ceramic additives are accompanied with silver coating, the resultant specific contact resistance is not much lower than the other two.

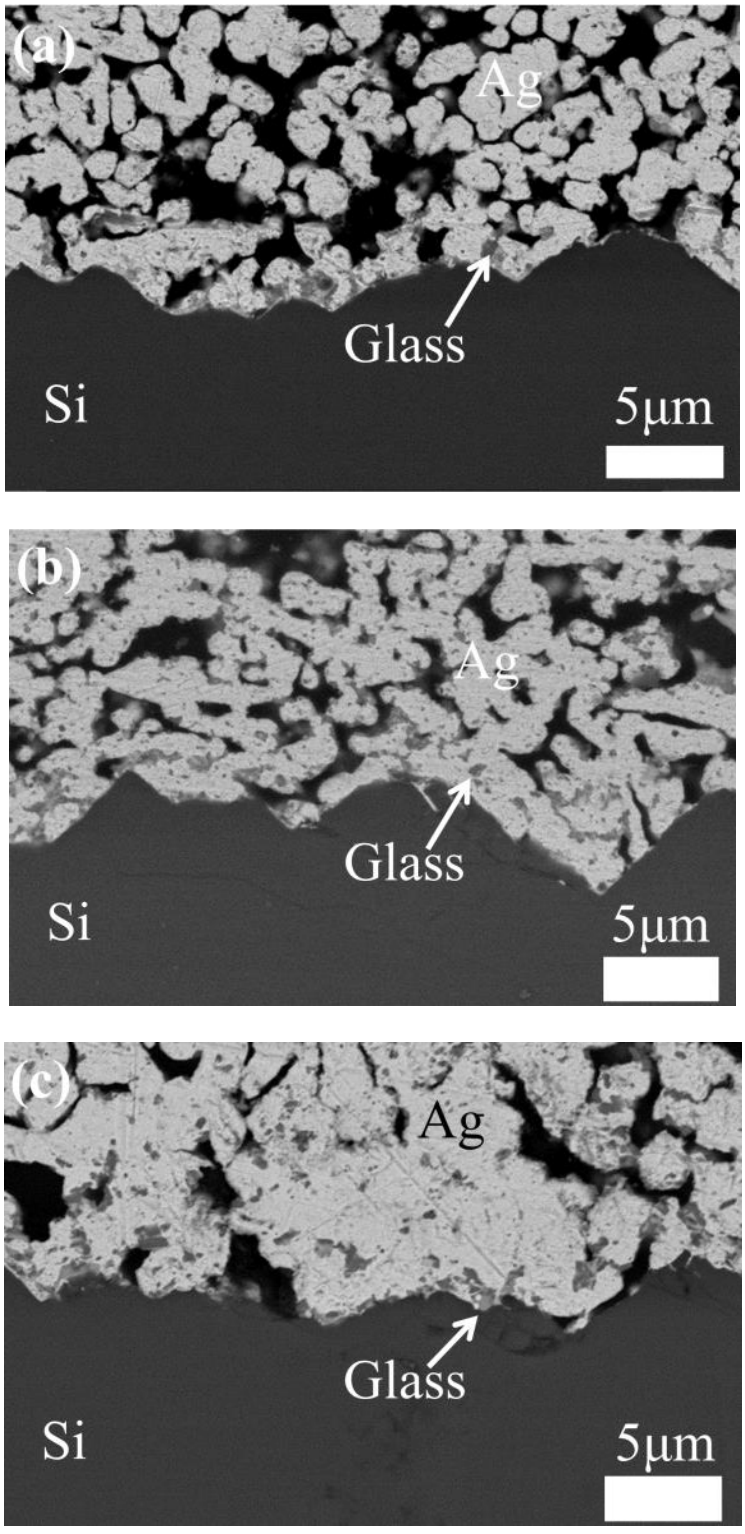

Fig. 3.3. SEM images of tested samples made with (a) N-1, (b) NE-1 and (c) NE-2

3.4 Conclusion

Nano-sized ceramic additives incorporated with silver coating by electroless plating was tested and compared with pure ceramic additives in terms of electrical performance. The results indicate that the formula consisting of silver-coated ceramic additives, as long as they are not the major etching agent, shows improved specific contact resistance. Since low specific contact resistivity of the silver metallization contact is the most desirable property and is strongly affected by the interfacial microstructure and firing conditions, silver pastes with surface-modified ceramic additives are proven to possess high etching rate of ARC layers and subsequently form a desirable interfacial microstructure, which results in the preferable low specific contact resistance. On the other hand, silver coating on the major etching agents actually reduce their etching ability, resulting in interface with higher contact resistivity. It is evident that with lower specific contact resistance, the overall efficiency of silicon photovoltaic cells will be higher under otherwise identical conditions due to the higher fill factor. The results of this present study demonstrate the importance of surface modification for chemical reactions, and also provide a new method for further enhancement in solar cell efficiency.

In this work, two activation and plating solutions with different concentrations are employed to study the influence of activation and plating steps in the electrical performance of resultant silver-coated nano-sized ceramic additives for silver metallization in crystalline silicon solar cells. It is found that with the diluted activation solution, silver plating with higher coverage can be achieved and therefore the resultant silver paste shows better electrical performance. Results from different plating conditions also indicate that the effect of concentration of plating solutions is minor as long as a sufficient plating duration is applied. Nanoparticles treated with the diluted activation solution form silver clusters with higher

coverage and therefore the result of silver blocking the connection between two adjacent ceramic additives is better. Although with longer activation time, the activation solution with the original concentration might achieve similar results as the diluted one does, the later one still show better performance due to the more uniform resultant silver coating layer it can achieve, and less compounds it requires.

References

[1]. Y. Zhang, Y. Yang, J. Zheng, G. Chen, C. Chen, J.C.M. Hwang, B.S. Ooi, A. Kovalskiy, and H. Jain, "Effect of the interface glass on electrical performance of screen printed Ag Thick-film contacts of Si solar cells", *Thin Solid Films* 518, e111-e113(2010).

[2]. S.B. Rane, T. Seth, G.J. Phatak, and D.P. Amalnerkar, "Effect of inorganic binders on the properties of silver thick films", *J. Mater. Sci.: Mater. Electron.* 15, 103 (2004)

[3]. Y.C Shih, Y.H. Lin, J.P. You and F.G. Shi, "Screen-Printable Silver Pastes with Nanosized Glass Frits for Silicon Solar Cells", *J. Electron. Mater.*, Vol. 42, No. 3 pp410-416 (2012).

[4]. A.S. Ionkin, B.M. Fish, Z.R. Li, M. Lewittes, P.D. Soper, J.G. Pepin, and A.F. Carroll, "Screen-Printable Silver Pastes with Metallic Nano-Zinc and Nano-Zinc Alloys for Crystalline Silicon Photovoltaic Cells", *ACS Appl. Mat. Interfaces*, 3, 606 (2011).

[5]. C.H Hsu, M.C Yeh, K.L. Lo, and L.J. Chen, "Application of Microcontact Printing to Electroless Plating for the Fabrication of Microscale Silver Patterns on Glass", *Langmuir*, 23, 12111-12118 (2007)

[6]. Y. Kobayashi, V. Salgueirino-Maceira, and L.M. Liz-Marzan, "Deposition of Silver nanoparticles on Silica Spheres by Pretreatment Steps in Electroless Plating", *Chem. Mater.*, 13, 1630-1633 (2001)

[7]. J. Choma, D. Jamiola, J. Ludwinowicz, and M. Jaroniec, "Deposition of silver nanoparticles on silica spheres and rods", *Colloid. Surface A*, 411, 74-79 (2012)

[8]. Dieter K. Schroder, *Semiconductor Material and Device Characterization, 2nd ed.* (New York: John Wiley & Sons, 1998), p. 156.

CHAPTER 4

ROLE OF TRANSPARENT DIE ATTACH ADHESIVES FOR ENHANCING LUMEN OUTPUT OF MID-POWER LED EMITTERS WITH STANDARD MESA STRUCTURE

4.1 Introduction

With the increased market penetration of solid state lighting in general illumination applications, high power LEDs have been developed rapidly in recent years. However, high power LEDs have several limitations including the light conversion efficiency and the redundant heat accumulation in LED packages. The improvement of epitaxial technology can reduce defect density and thus decreases nonradiative recombination of carriers [1]. The textured or rough LED chip surfaces increase light extraction efficiency from semiconductor [2]. Significant advances in chip-level design has been reported for GaN-based LEDs, mostly are to reduce the "efficiency droop" [3-5], including the incorporation of quantum wells with large overlap to suppress the charge separation [5], the use of wide double-heterostructure active regions to reduce Auger recombination issue [6], the reduction of polarization effect within the multiple-quantum well region to minimize the electron leakage, and new barrier designs to suppress the efficiency droop issue [7, 8]. Packaging technologies and materials also hugely affect the light extraction efficiency [9-12] and there are continuously advancements in LED packaging materials and technologies, including the addition of backside reflector, novel chip surface optical structures for light extraction and new packaging methods, which include multi-

layered phosphor for white LEDs [9], new reflector cup materials [13], and new encapsulation materials with improved thermal and radiation resistance [14]. However, there is still an excess amount of undesired heat generated inside the LED package because the light conversion efficiency of high power LEDs is still lower than 35%. This leads to an increase in the junction temperature of LEDs. The increased junction temperature adversely decreases the light output and life span of LEDs. On the other hand, mid- and low-power LEDs provides less expensive option in comparison with high-power LEDs, easier thermal management because they generate less heat, and also better light output control, in terms of both brightness and light uniformity. Mid-power white LED emitters (30 to 150 mA input current) based on sapphire substrate with standard MESA structure are currently the dominant LEDs for LCD BLU applications, and they also appear to dominate general lighting applications.

Although the optical impact of the essential packaging materials, such as encapsulant and the reflector cup, is evident and has been well studied as well [14], no study has been reported on the optical performance of DAAs on either monotonic color LED or white LED emitters. This is probably because the extreme small amount (less than 10 mg) of DAA used for attaching one LED die onto the substrate. Thus the objective of the present work is to study the role of DAAs in influencing the lumen output of both blue and white LEDs under different conditions. It is established for the first time that a replacement of conventional silver-filled epoxy DAA by an optically transparent DAA can lead to a significant enhancement of light output: as high as 13% increase for mid-power blue LEDs with about 40% fillet coverage, and 21% increase for white LEDs. The mechanism for the observed enhancement is discussed.

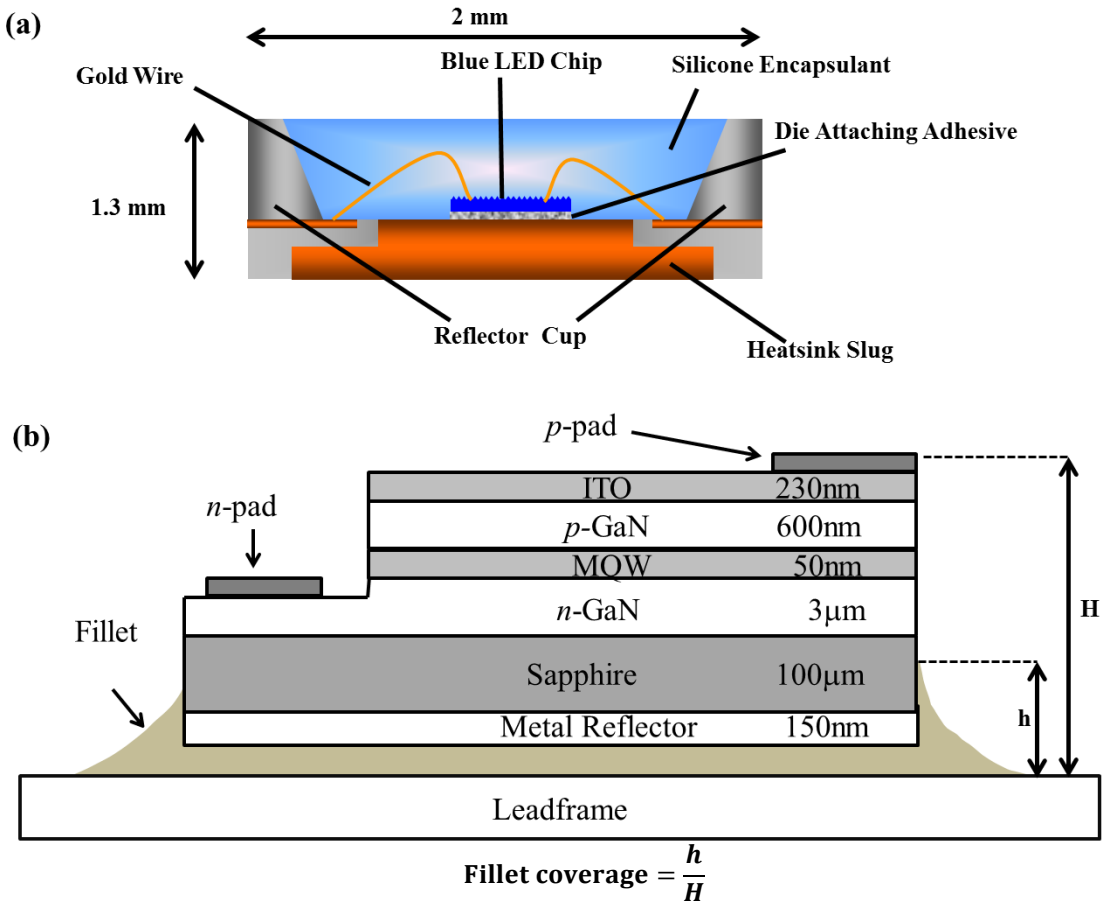

Fig. 4.1. (a) Schematic drawing of a cross-sectional view of a 0.5 W monochromatic blue LED package with pure silicone encapsulant; (b) a macroscopic enlargement of the chip and the DAA layer.

Table 4.1 Optical properties and curing conditions of two different DAAs used in this work.

	Appearance	Curing Condition	Absorptance @450nm*
OC-DAA	Translucent	2 hours @ 150℃	15%
Ag-DAA	Silver	45 mins @175℃	73%

*Sample thickness: 1mm

4.2 Experimental

The schematic drawing of a packaged 0.5W blue LED emitter is illustrated in Fig. 4.1 (a) and it is comprised of a leadframe with a reflector cup, an LED chip, a die attach adhesive, gold wires and silicone encapsulant. The refractive index of the silicone encapsulant used in this study is 1.53. Two DAAs were used as die bonding materials. One is an optically transparent clear DAA (denoted as OC-DAA) formulated by Shi's lab [14] and the other one is commercially available conventional silver-filled epoxy DAA (denoted as Ag-DAA). The optical properties of these two DAAs are summarized in Table 4.1. For white LED emitters used in the experiment, the silicone mixed with 7.5 wt.% of yellow phosphor powder was used as the encapsulant material and the resulted CCT is about 9200 K. In this work, commercially available 0.5 W parallel type LED chips with standard MESA structure on sapphire substrate were used, as schematically shown in Fig. 4.1(b). The peak wavelength of these LED chips is 450 nm. The most important processing parameter for die attach operation is the DAA fillet around the chip, as schematically shown in Fig. 4.1(b). Packaged samples with different fillet coverage were obtained by precisely controlling the amount of DAAs. Fillet coverage was measured with an optical microscope before wire-bonding to avoid image distortion caused by the silicone encapsulant if measured after encapsulation. Covered area of DAA materials on all four sidewalls in one chip was measured and the fillet coverage was obtained by dividing the total covered area by the total area of four sidewalls. Figure 4.2 demonstrates how DAA materials interact with different emitted photons in the leadframe cavity [15, 16]. Path A shows the path of light escaping from the cavity after the light goes through either path B or C. The fillet coverage in this illustration is about 40% which is the value employed in the regular LED packaging process. A too lower fillet will probably result in insufficient adhesion strength and the chip will

detach from the leadframe due to the thermal stress arisen during operation. A too higher will cause two issues: first if the DAA is not optically transparent, the fillet will block the emitted photons, as path B shown in Fig. 4.2. If the DAA is electrically conductive and is close to the electrodes on the upper chip surface, an electrical short circuit might take place which leads to failure of the entire device. The DAA fillet around the LED chip can be observed after the first curing process list below. The packaging process is as follows: (1) the leadframe (Techwin 2027, 2.7 mmX2.0 mmX1.3 mm) used in this experiment is by Techwin Opto-Electronics and is cleaned by isopropyl alcohol and baked at 80 ℃ prior to use; (2) the blue LED chip is attached to the center of the reflector cup of the leadframe by using a die attaching adhesive; (3) the samples are then cured with the curing conditions shown in Table 4.1; (4) wire-bonding is performed to electronically connect the LED chip to the leadframe; (5) silicone encapsulant is dispensed into the cavity of the reflective cup to encapsulate the LED chip; (6) the samples then are cured at 150℃ for 2 hours; (7) the packed LED is soldered to an Al-based printed-circuit-board.

The current source with corresponding indicated forward voltage was supplied by Everfine power generator. The constant current used for the measurement is 150 mA. The light output of LEDs was measured in a LabSphere integral sphere. Transmittance was measured by GENESYS 20 spectrophotometer by Thermo Electron Corporation. Reflectance measurements were carried out with IS-1 integrating sphere by Filmetrics. Thickness of samples for transmittance and reflectance measurements is 1 mm. Absorptance was then calculated by subtracting transmittance and reflectance from 100%. The method employed to measure the junction temperature is as described in the references [13] and is measured under natural convection condition. Simulation analysis was carried out with LightTools (Synopsis) and the results were used to compare with the experimental data acquired from the optical measurement. The

simulated device structure is the same as shown in Fig. 4.1 (a) and the 2027 leadframe used in the experiment. The optical properties of two different DAAs for the simulation are also the same as those of the DAA materials applied in this work.

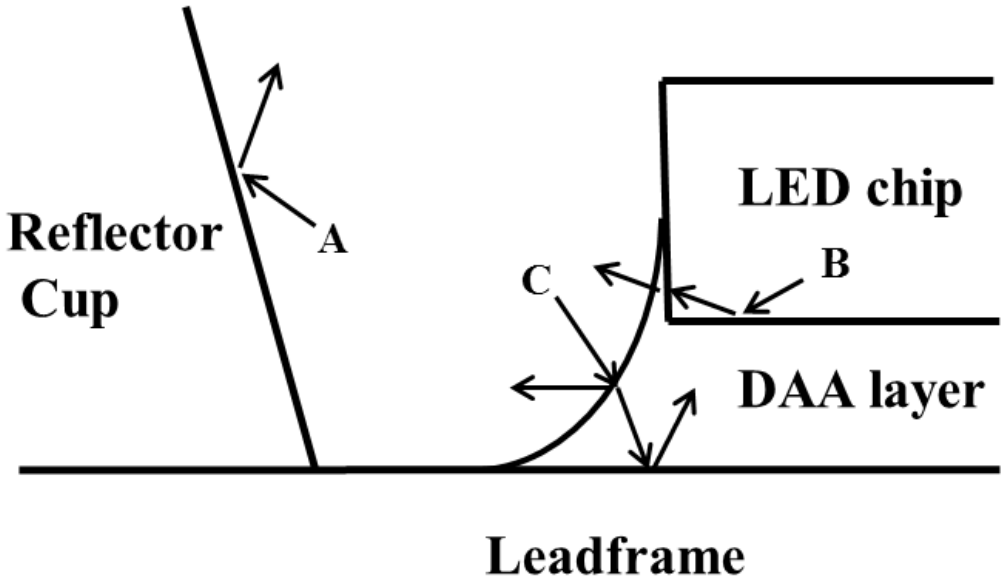

Fig. 4.2. An illustration shows how different DAAs affect the optical output of the packaged blue LED. A, B and C represent three possible light paths.

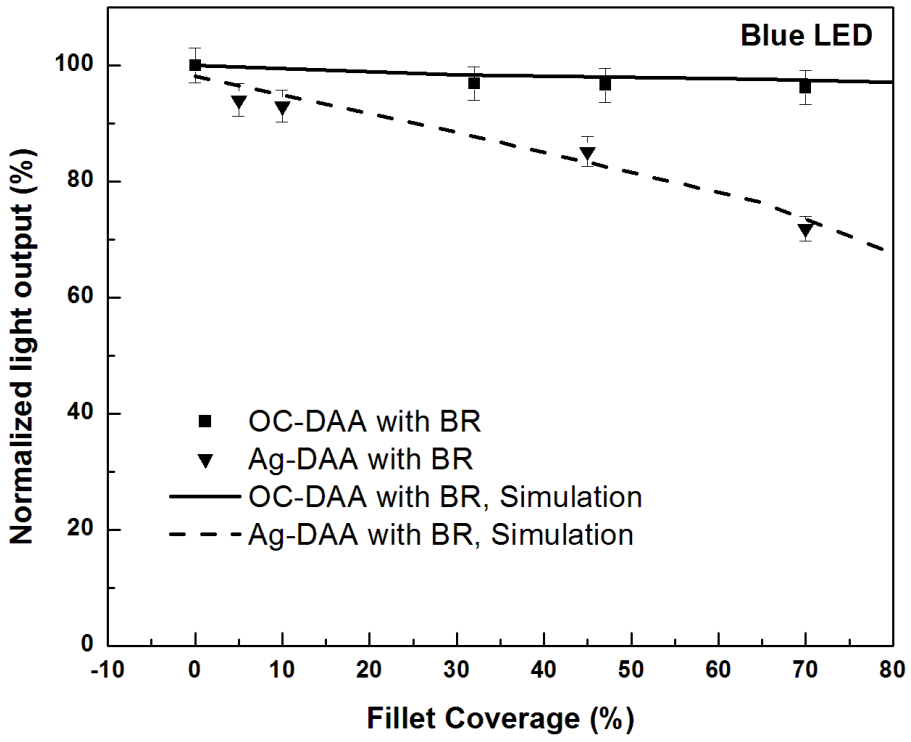

Figure 4.3. Light output of 0.5 W blue LED emitters with a backside reflector (BR) encapsulated with pure silicone as a function of DAA fillet coverage. The optically clear silicone-based DAA is denoted as OC-DAA and the commercial silver-filled epoxy DAA is denoted as Ag-DAA. The solid line is simulation result for OC-DAA and the dash line is for Ag-DAA.

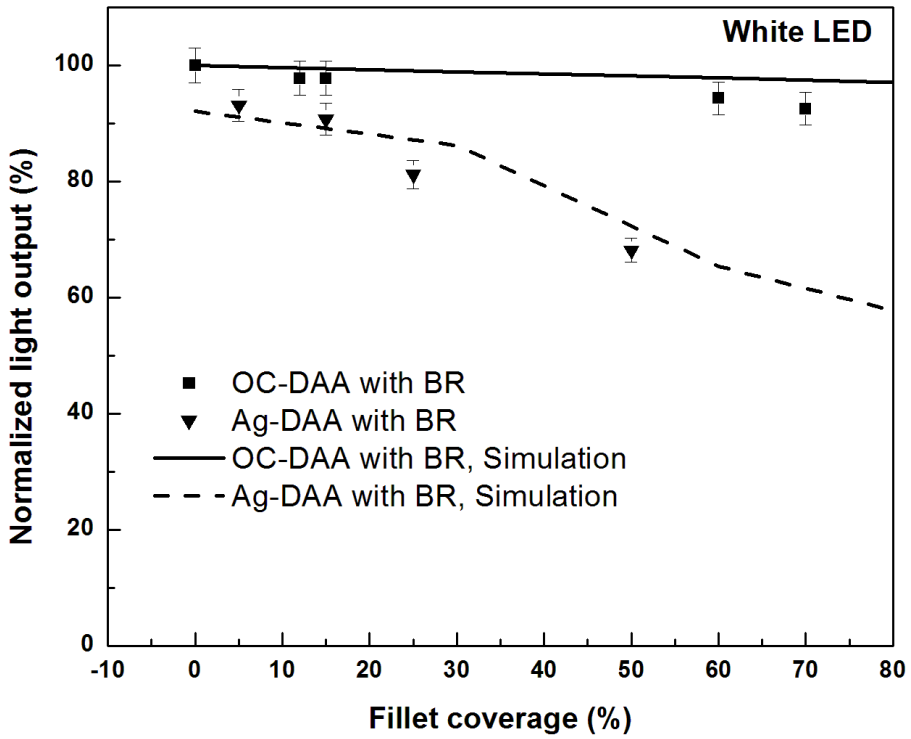

Figure 4.4. Light output of 0.5 W white LED emitters with BR, as a function of DAA fillet coverage. The emitters are encapsulated with silicone and 7.5 wt% yellow phosphor powder.

4.3 Result and Discussion

Light output of LEDs as a function of fillet coverage with two different DAAs is shown in Fig. 4.3. In Fig. 4.3 the solid line is the simulation result for the optically transparent clear DAA, which is denoted as OC-DAA and the dash line is for the commercial silver-filled epoxy DAA, which is denoted as Ag-DAA. In Fig. 4.3 optical output of the samples packaged with OC-DAA and 0% fillet coverage is set as 100% for comparison. From the results it shows that for samples packaged with OC-DAA, the optical output only slightly decreases as the fillet coverage increases. However for the samples packaged with Ag-DAA, light output decreases significantly as the fillet coverage increases. This result can be interpreted by the illustration shown in Fig. 4.2 and the different absorptance of two DAAs shown in Table 4.1. For light path B in Fig. 4.2, the difference between different DAAs is small with low fillet coverage because the DAA fillet covering the side of the LED chip is very thin and therefore the influence of DAAs is negligible. But the absorptance of photons at the interface between the sidewall of chip and the DAA fillet is expected to increase if the fillet coverage increases, especially for the Ag-DAA which has a higher absorptance. Although the side area is small, the photon density is much higher due to the reflected light from the metal reflector. There is a large portion of photons emitted downward from the emitting layers and the metal reflector on the bottom of the chip can reflect the light back to the upward direction. If more photons can escape from the side of the chip, then the light extraction can be furthermore increased. However if the die attaching material on this section blocks or absorbs photons, it leads to a loss in the overall light extraction efficiency. The fillet also extends and covers the surrounding area near the LED chip so from the top view it looks like a frame around the chip. This will also increase the interaction area between the die attaching materials and the emitted photons.

Light path C in Fig. 4.2 shows another possible route of photons travelling within the cavity before they are absorbed or leave the cavity. At the surface of the DAA fillet, absorption, transmission and reflection will happen. For OC-DAA, most of the photons will transmit through the interface and then come out from the other side of the DAA layer. However if Ag-DAA is selected instead, most of the photons will be reflected or absorbed at the fillet surface. Therefore even with 0% fillet coverage, optical output of the samples packaged with Ag-DAA is still slightly less than that of the samples packaged with OC-DAA because the absorption happens on the surface of Ag-DAA on the bottom around the chip. With higher fillet coverage the amount of photons moving similar paths to path C will also increases. The above discussion explains the different behavior of two DAAs on optical output as a function of fillet coverage shown in Fig. 4.3. For fillet coverage at 40%, the difference from two different DAAs is about 13%, which is a huge loss for a package employing conventional DAA as the die bonding material. For a 0.5 W packaged blue LED emitters with Techwin 2027 leadframe, the surface area of die attaching materials with 40% fillet coverage is only about 2% of total reflecting surface area within the reflector cup but from the experimental result it is demonstrated that with different die bonding materials selected for the packaging process, how enormous the impact on optical performance is from the 2% area.

Figure 4.4 is the result of white LEDs as a function of fillet coverage from samples packaged with two different DAAs. For white LEDs, the optical output is expressed in lumen per input power so the unit is lm/W. In order to do the comparison better, a normalized optical output is applied in this figure as well and optical output of the samples with OC-DDA and 0% fillet coverage is set to be 100%. With addition of 7.5 wt.% yellow phosphor, the measured CCT is about 9200 K. The results of optical output are similar with those from blue LEDs but the

difference between two different types of DAAs as the fillet coverage increases becomes larger for white LEDs. For 40% fillet coverage, the difference in optical output is about 21% and it becomes larger when fillet coverage increases. The reason of this value being higher than that of blue LEDs with the same fillet coverage is because the effect of photon scattering from the phosphor particles inside the encapsulant, which provides extra chance for the converted photons to be absorbed by the DAAs if they are scattered backward to the bottom of the leadframe [15, 16]. Figure 4.5 shows the absorptance of DAA materials in the visible wavelength range and a absorptance more than 55% in this range is observed for this material. Because the absorptance of Ag-DAA is much higher than that of OC-DAA, this effect of back-scattering of photons causes the loss of light extraction in these samples to be larger.

Figure 4.6 (a) shows the change in junction temperature versus time for blue emitters made with two different DAAs. The result shows that although samples with blue emitters exhibit lower junction temperatures, the difference between two DAAs is less than two degree Celsius or 1% of the total temperature. Figure 4.6 (b) shows the normalized light output versus time for the same samples in Fig. 4.6 (a) and the instantaneous light output is used as 100% reference for samples with different DAAs. This result shows after turning on for about 10 minutes, samples made with different DAAs show similar trend in light output degradation and the drop percentage is very close for both types of samples although their initial light output is different. The result from the junction temperature measurement and normalized light output in different time intervals elucidates that with lower requirement of heat dissipation for mid-power LEDs, OC-DAA with lower thermal conductivity shows similar thermal performance to Ag-DAA whose thermal conductivity is about ten times larger. Therefore for mid-power LEDs,

different materials with similar optically transparency can be applied to achieve optical performance similar with the OC-DAA used in this work.

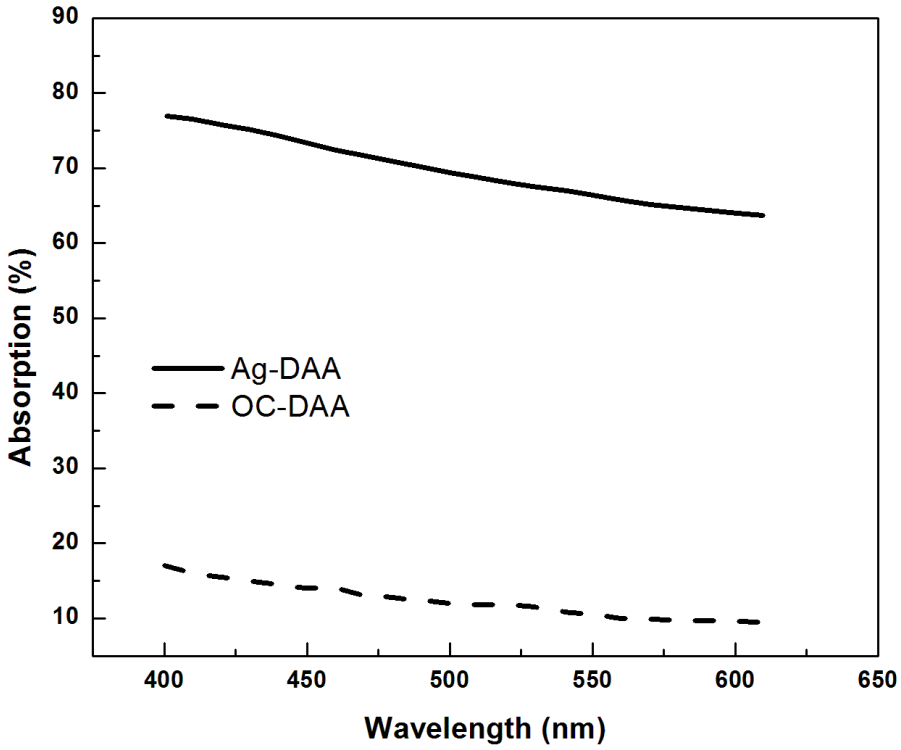

Figure 4.5. Absorptance of DAA materials used in this work. Thickness of tested samples is 1 mm.

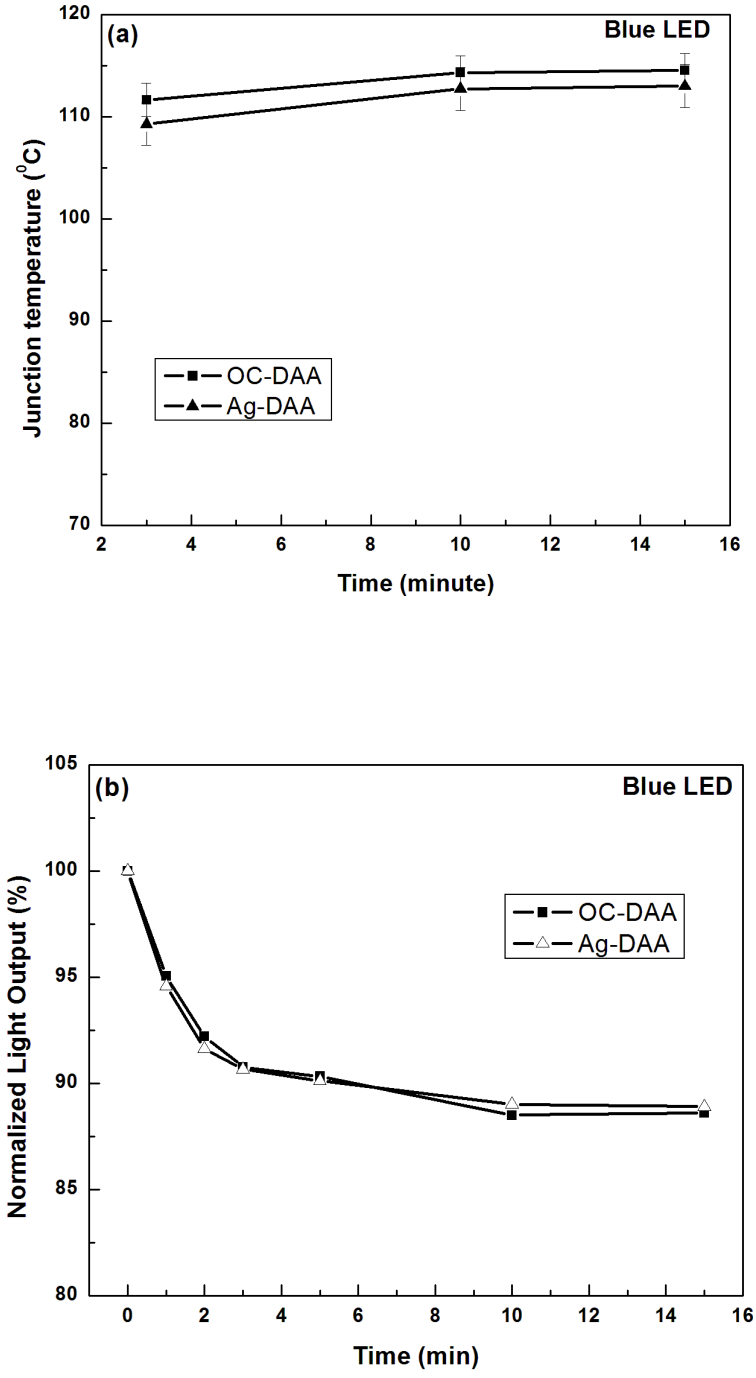

Figure 4.6. (a) Junction temperature and (b) normalized light output versus time for the tested 0.5 W blue LED samples packaged with different DAAs.

4.4 Conclusion

In this work, optical measurement was performed for samples packaged with two different types of DAAs and the optical impact on light extraction efficiency of packaged LED emitters with different DAAs is presented for the first time. It is found that such an optical impact is enormous when the transparent adhesive is employed and a 21% difference in optical output is observed between conventional silver-filled epoxy DAA and optically clear silicone based DAA used for die-bonding of white LED packaging. This better performance of LEDs packaged with optically clear DAA is due to the low absorptance of the die bonding material which causes less loss when photons emitted from the emitting layer interact with the die bonding material around the chip. The measurement of junction temperature on different emitters also suggests that optically clear DAA has similar thermal performance to conventional silver-filled epoxy DAA for mid-power LEDs and it is expected that the result should be the same for low-power LEDs. Although conventional silver-filled epoxy DAAs still have the advantage of high thermal conductivity, for mid- and low-power LEDs which have less requirements for heat dissipation, optically clear DAAs might be a better choice for its sufficient thermal dissipation ability and excellent light extraction efficiency. It is also predictable that optically clear type DAAs will replace the conventional silver-filled DAAs for use in high-power LEDs when their thermal conductivity is promoted to a higher level.

References

[1]. Kirchner, C, "Homoepitaxial growth of GaN by metalorganic vapor phase epitaxy: A benchmark for GaN technology," *J. Appl. Lett.,* Vol. 75 (8), pp. 1098-1100 (1999).

[2]. Windisch, R, "Light-extraction mechanisms in high-efficiency surface-textured light-emitting diodes," IEEE J. Selected Topics Quantum Electronics, Vol. 8, pp. 248-255 (2002).

[3]. J. Piprek, "Efficiency droop in nitride-based light-emitting diodes", *Phys. Status. Solidi. A*, Vol. 207, No. 10, pp. 2217-2225 (2010)

[4]. M.H. Kim, M.F. Schubert, Q. Dai, J.K. Kim, E.F. Schubert, J. Piprek and Y. Park, "Origin of efficiency droop in GaN-based light-emitting diodes", *Appl. Phys. Lett.*, 91, 183507 (2007)

[5]. D.F. Feezell, J.S. Speck, S.P. DenBaars and S. Nakamura, "Semipolar (20-2-1) InGaN/GaN Light-Emitting Diodes for High-Efficiency Solid-State Lighting", *J. Disp. Technol.,* vol. 9, No. 4, pp. 190-198 (2013)

[6]. N.F. Gardner, G.O. Muller, Y.C. Shen, G. Chen, S. Watanabe, W. Gotz and M.R. Krames, "Blue-emitting InGaN-GaN double-heterostructure light-emitting diodes reaching maximum quantum efficiency above 200 A/cm^{2}", *Appl. Phys. Lett.,* 91, 243506 (2007)

[7]. S. Choi, M.H. Ji, J. Kim, H.J. Kim, M.M. Satter, P.D. Yoder, J.H. Ryou, R.D. Dupuis, A.M. Fischer and F.A. Ponce, "Efficiency droop due to electron spill-over and limited hole injection in III-nitride visible light-emitting diodes employing lattice-matched InAlN electron blocking layers", *Appl. Phys. Lett.*, 101, 161110 (2012)

[8]. G. Liu, J. Zhang, C.K. Tan and N. Tansu, "Efficiency-Droop Suppression by Using Large-Bandgap AlGaInN Thin Barrier Layers in InGaN Quantum-Well Light-Emitting Diodes", *IEEE Photonic. Tech. L.*, vol. 5, No. 2, 2201011 (2013)

[9]. J.P. You, N.T. Tran, F.G. Shi, "Light extraction enhanced white light-emitting diodes with multi-layered phosphor configuration", *Opt. Express*, vol. 18, No. 5, pp. 5055-5060 (2010).

[10]. V.R. Manikam, K.Y. Cheong, "Die attach materials for high temperature applications: a review", *IEEE Trans. Compon. Packag. Manuf. Tech.*. vol. 1, No. 4, pp. 457-478 (2011).

[11]. H.H. Kim, S.H. Choi, S.H. Shin, Y.K. Lee, S.M. Choi, S. Yi, "Thermal transient characteristics of die attach in high power LED PKG", *Microelectron. Reliab.*, 48, pp. 445-454 (2008).

[12]. J.K. Kim, H. Luo, E.F. Schubert, J. Cho, C. Sone, Y. Park, "Strongly Enhanced Phosphor Efficiency in GaInN White Light-Emitting Diodes Using Remote Phosphor Configuration and Diffuse Reflector Cup", *Jpn. J. Appl. Phys.*, vol. 44, No. 21, pp. L649-L651 (2005).

[13]. B. Yan, J.P. You, N.T. Tran, Y. He, F.G. Shi, "Influence of die attach layer on thermal performance of high power light emitting diodes", *IEEE Trans. Compon. Packag. Manuf. Tech.*, vol. 33, No. 4, pp. 722-727 (2010).

[14]. Y.H. Lin, J.P. You, Y.C. Lin, N.T. Tran, F.G. Shi, "Development of high-performance optical silicone for the packaging of high-power LEDs", *IEEE Trans Compon. Packag. Manuf. Tech.*, vol. 33, No. 4, pp. 761-766 (2010).

[15]. S.L. Hsiao, N.C. Hu, H. Cornelissen, “Phosphor-converted LED modeling using near-field chromatic luminance data”, *Opt. Express*, vol. 21, issue S2, pp. A250-A261 (2013)

[16]. N. Narendran, Y. Gu, J.P. Freyssinier-Nova, Y. Zhu, “Extracting phosphor-scattered photons to improve white LED efficiency”, *Phys. Stat. Sol.(a)*, 202, No. 6, pp. R60-R62 (2005)

CHAPTER 5

NOVEL OPTICALLY REFLECTIVE DIE BONDING ADHESIVE FOR MESA TYPE LIGHT-EMITTING DIODES: OPTICAL AND THERMAL PERFORMANCE

5.1 Introduction

The MESA type low-to-mid power GaN-based light emitting diodes (LEDs) are the mainstream chips used in general lighting and liquid crystal display backlighting applications, mainly because of their cost-performance effectiveness [1-4]. While the chip quantum efficacy has been greatly improved [5-8], it is only recently realized that a replacement of conventional silver-based die attach adhesives (DAAs) by an optically clear DAA leads to a great enhancement (as high as 13%) of light output for the packaged monochromatic LED emitters [4], although the DAA amount needed for each emitter is only a few fractions of a microgram. An optically clear DAA often has a thermal conductivity of less than 0.2 W/mK, which is much lower than the thermal conductivity of 2 W/mK for a typical silver DAA (Ag-DAA). There is evidently a need for developing a novel DAA material with not only better optical effect than Ag-DAAs, but with a comparable thermal performance in terms of bondline thermal resistance.

Thus, the objective of this work is to demonstrate such a novel die bonding DAA for standard MESA type LEDs. It is shown this new DAA can not only have a greatly enhanced light output than a typical Ag-DAA, but also can lead to a lower thermal resistance, a reduced junction temperature and thus an enhanced light output lifetime performance.

5.2 Experimental

The packaged monochromatic LED emitter (with a dominant wavelength at 450nm) is comprised of a 5050 leadframe (5x5x1.3 mm) with a reflector cup, an LED chip, a die attach adhesive, gold wires and silicone encapsulant with an index of refraction equal to 1.53 at the wavelength of 450 nm. Figure 5.1 illustrates the schematic drawing of a typical packaged monochromatic LED emitter. In order to present each layer more clearly and emphasize the important layers, layers in Fig. 5.1 (b) are not plotted in their relative thickness. The value of thickness of different layers might be varied based on different designs of LED chips. The monochromatic LED emitter used in this work is operated at constant current mode (I = 350 mA) with a forward voltage equals to 3.3 V, and the size of the chips is 45x45 mil with a total thickness about 155 μm.

Two DAAs are employed in this study. The first one is a conventional silver-filled epoxy DAA (denoted as Ag-DAA) and the other one is the optically reflective white DAA (denoted as WDAA). The WDAA used in this work is consisting of 30 wt.% of 1μm TiO_2 powder and a high performance silicone [9]. Important properties of these two DAAs are summarized in Table 5.1, which demonstrates that the WDAA has similar adhesion strength but more excellent reflectance than the Ag-DAA.

The complete packaging process is as follows: (1) the 5050 leadframe (5x5x1.3 mm) used in this experiment is cleaned by isopropyl alcohol and baked at 80 ℃ before used; (2) the blue LED chip is attached to the center of the leadframe by using a die attaching adhesive, and WDAA samples with different bondline thickness were obtained through different applied bonding forces; (3) the samples are then cured at 150 ℃ for 2 hours; (4) wire-bonding is performed to electronically connect the LED chip to the leadframe; (5) silicone encapsulant with and without

phosphor is poured into the cavity of the reflective cup to encapsulate the LED chip; (6) the samples then are cured at 150 ℃ for 2 hours; (7) The packaged LEDs are then soldered to Al-based printed-circuit-board (PCB). In order to avoid the image distortion caused by the silicone encapsulant, the measurement of DAA fillet coverage is conducted with an optical microscope after the first curing step listed above [4].

Power generator by Everfine with constant current mode was used for this work and the value of the current was 350 mA. Light output of packaged LED emitters was measurement in a LabSphere integral sphere. Reflectance in Table 5.1 was measurement with IS-1 integrating sphere by Filmetrics. Thermal conductivity measurement was carried out by hot plate method. Thickness of samples for both thermal conductivity and reflectance measurement is 1 mm and the diameter is 25.4 mm. Scanning electron microscopy (Philips XL-30 FEG) was employed to investigate the bondline thickness. Junction temperature was carried out with the forward voltage method [10]. The reliability test was carried out in a temperature-humidity reliability testing chamber (model GLMP50 by Chemkorea Corporation) with operation conditions at 85℃ and 85% relative humidity.

Table 5.1. Physical and mechanical properties of two different DAAs used in this work.

	Appearance	Reflectance @450 nm*	Thermal Conductivity (W/mK)*	Lap Shear Strength (MPa)**
WDAA	White	92%	0.88	10.61
Ag-DAA	Silver	27%	2.40	10.24

*Sample thickness: 1 mm

**Attaching area: 5 mm x 25 mm; DAA thickness: 80 μm

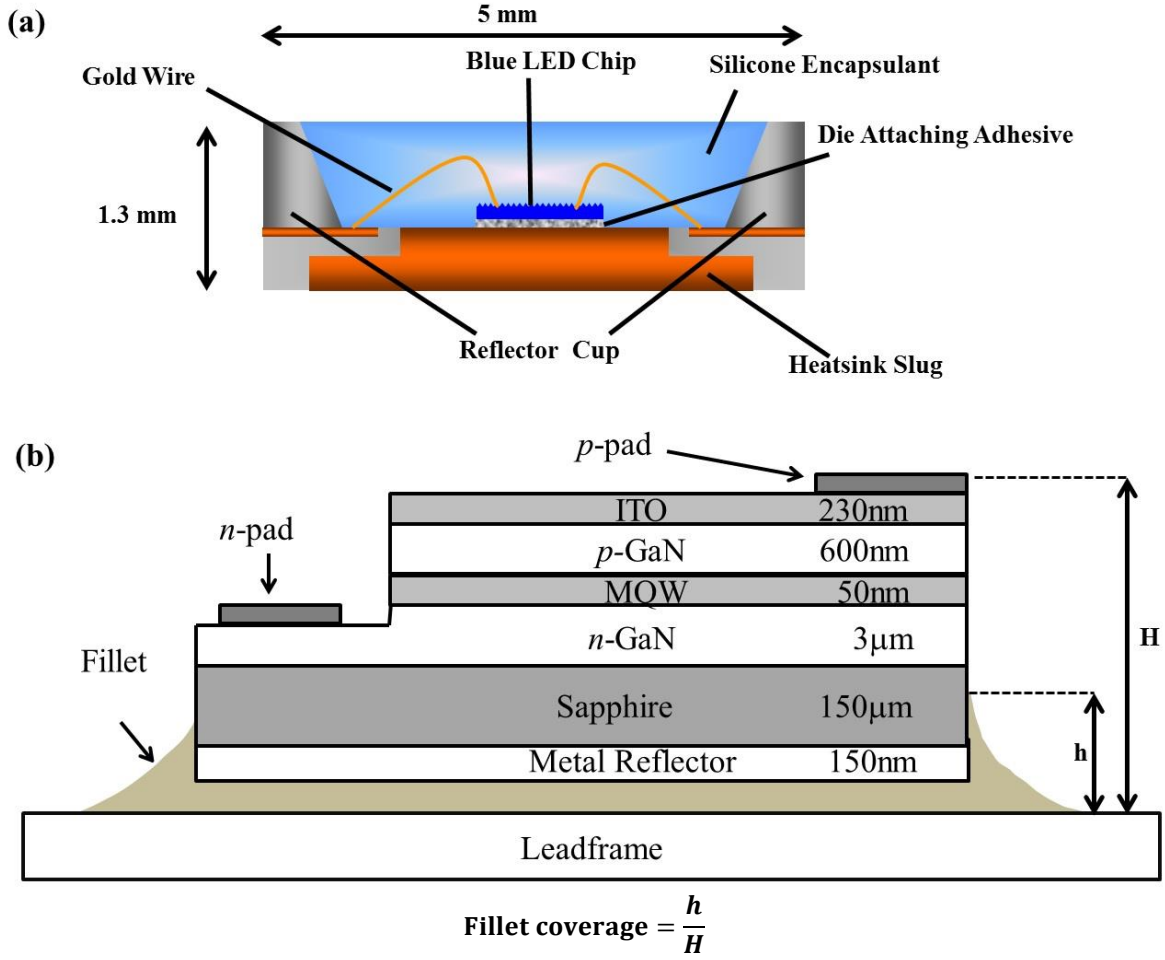

Figure 5.1. (a) Schematic drawing of the cross-sectional view of a monochromatic blue LED package with silicone encapsulant; (b) a macroscopic enlargement of the chip and the DAA layer.

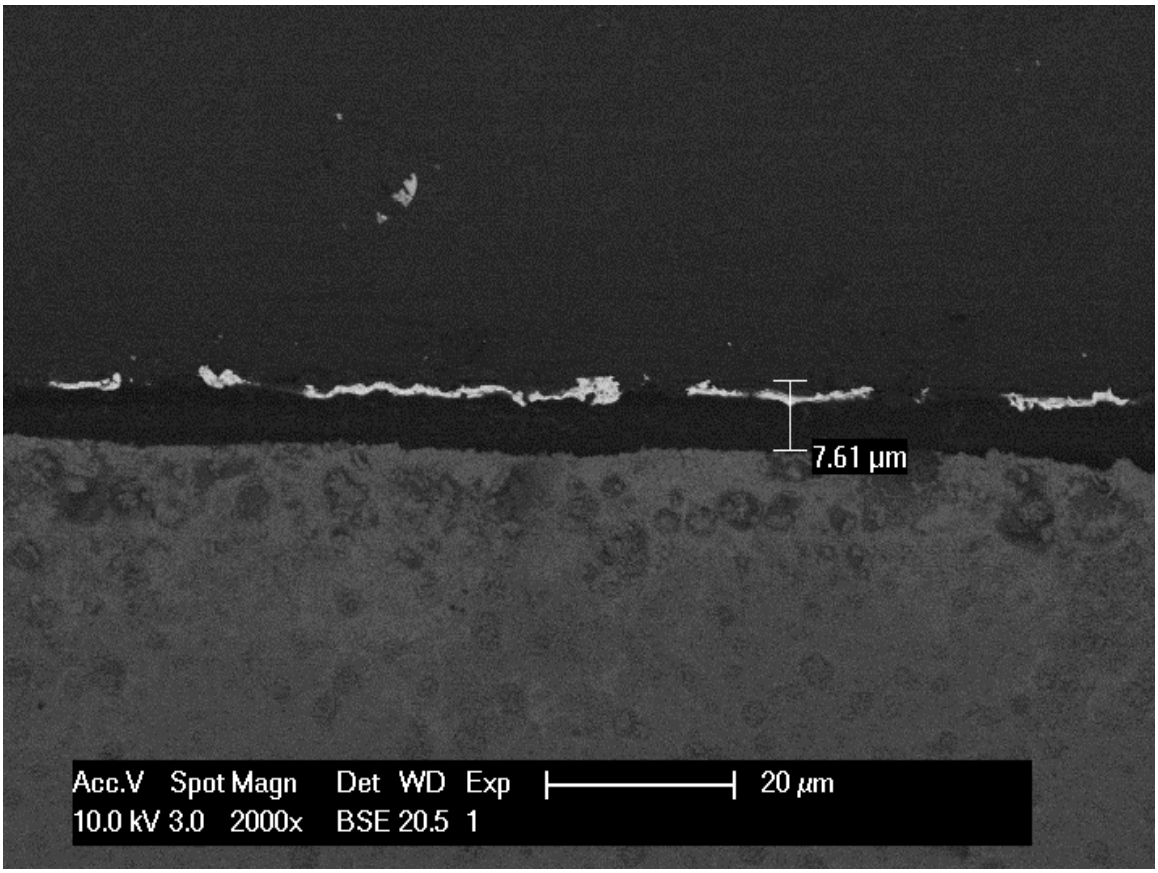

Figure 5.2. The SEM BSE image of the WDAA sample with bondline thickness of 7.61 µm.

5.3 Results and Discussion

Figure 5.2 shows the SEM BSE image of a WDAA sample with 7.6μm BLT and Fig. 5.3 is the result of normalized instantaneous measurement for 1 W (I=350 mA and V=3.3 V) monochromatic LED emitters packaged with two different DAA materials, and fillet coverage for all samples is 40%. The BLT value for Ag-DAA samples is 20 μm and for WDAA samples is 7.6 and 20 μm. Radiation output from WDAA samples with 20 μm is set as reference for comparison. From Fig. 5.3 it shows that the difference in radiation output between WDAA samples with different BLT values is negligible, and WDAA samples exhibit 11% higher than Ag-DAA samples. For WDAA samples, the effect of BLT on radiation output is small because WDAA is a diffuse reflector, and the reflection takes place only on the surface of WDAA layers [11]. On the other hand, Ag-DAA shows high absorptance at 450nm, and the drop in radiation output is large [4].

Figure 5.4 shows the results of normalized instantaneous measurement for 1 W (I=350 mA and V=3.3 V) monochromatic LED emitters packaged with WDAA and Ag-DAA. Radiation output of WDAA samples with 20 μm BLT and 0% fillet coverage is set as reference in this figure. In fig. 5.4, both WDAA samples show almost no difference in radiation output at different fillet coverage. All three samples exhibit high radiation output at low fillet coverage and then decreases while fillet coverage increases. At 0% fillet coverage, the difference in light output between two different DAAs is only about 1% but Ag-DAA samples experience higher drop at high fillet coverage. At 40% fillet coverage, the difference in radiation output between two different DAA becomes 11%. When the fillet coverage is low, the difference in radiation output is small because the chance for photons to be absorbed is limited, especially for Ag-DAA materials due to small exposed surface area. The drop in radiation output for WDAA samples

after 40% fillet coverage and in Ag-DAA after 10% fillet coverage is due to the side-wall blocking by the DAA materials [4]. For WDAA samples, this drop is smaller and postponed to higher fillet coverage because WDAA materials do not absorb extensive photons and therefore after multiple scattering within the DAA layers, incident photons can still escape. When fillet coverage reaches 40% in WDAA samples, the side wall becomes thick enough and therefore the window for photons to escape becomes much smaller and a significant drop is observed. For Ag-DAA materials, a large portion of incident photons are absorbed by the DAA layer, the drop in radiation output is much larger than that of WDAA at the same fillet coverage.

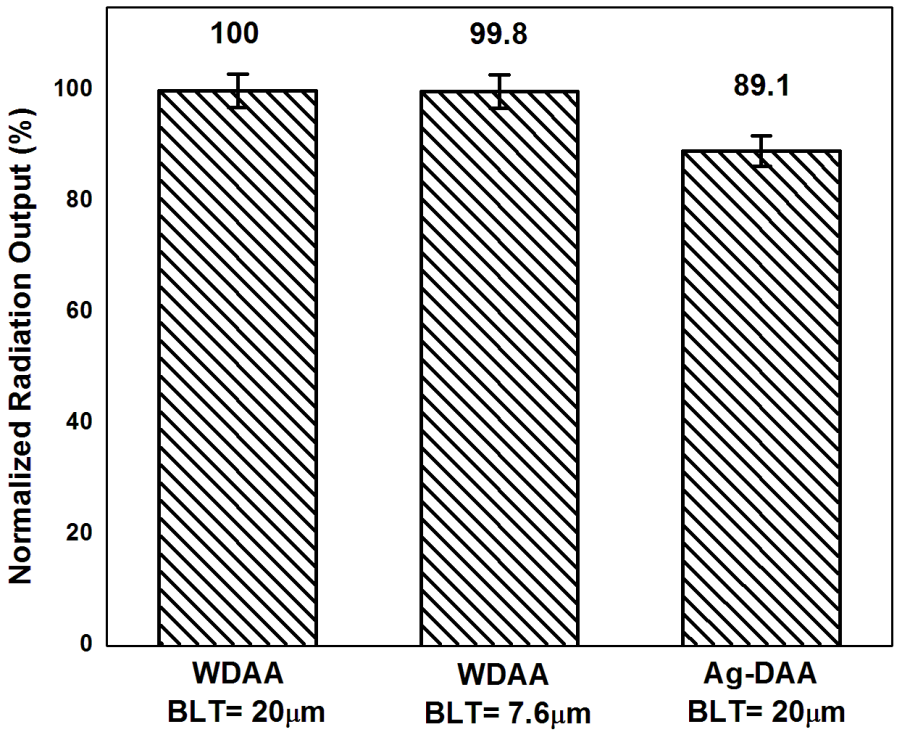

Figure 5.3. Normalized instantaneous radiation output of 1 W (I=350 mA and V=3.3 V) monochromatic LEDs packaged with different DAA materials and encapsulated with silicone. The bondline thickness (BLT) for Ag-DAA samples is 20 μm and for WDAA samples is 20 and 7.6 μm. Radiation output from WDAA samples with 20 μm BLT is set as 100% for reference and fillet coverage for all samples is 40%.

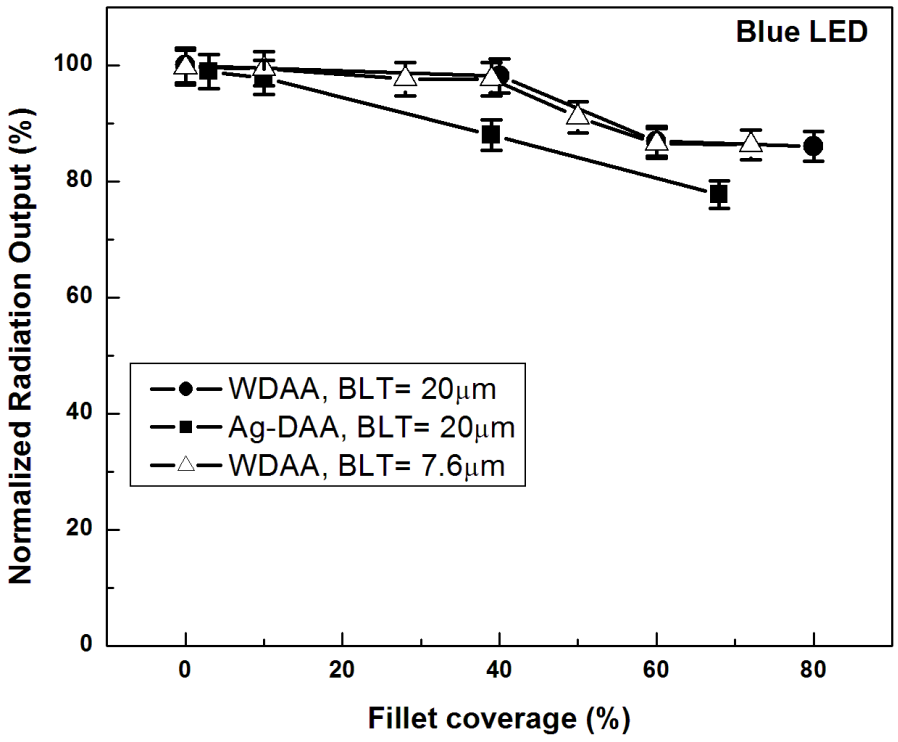

Figure 5.4. Normalized instantaneous radiation output of 1 W (I=350 mA and V=3.3 V) monochromatic LED emitters packaged with different DAA materials and encapsulated with silicone, as a function of DAA fillet coverage. The BLT for Ag-DAA samples is 20 μm, and for WDAA samples are 20 μm and 7.6 μm. Radiation output from 0% fillet-covered WDAA samples with 20 μm BLT is set as 100% for reference.

Figure 5.5 is the normalized steady-state radiation output, as a function of time, for Ag-DAA with 20 μm BLT and WDAA with 20 and 7.6 μm BLT. In this figure all three samples are set as 100% initially to show the difference between different samples. The optical measurement shows a significant drop in radiation output for all samples before 180 seconds, and then it becomes steady after 600 seconds. From the results it shows that the WDAA sample with 7.6 μm BLT exhibits a weaker drop at the first 180 seconds after the power is on, and also a smaller degradation in optical output during the entire operation.

Figure 5.6 is the result of junction temperature measurement obtained with the forward voltage method, on samples packaged with different DAA materials, as a function of operation time. Fillet coverage for all tested samples is 40%. For Ag-DAA, BLT is 20 μm and for WDAA, two different BLT values (20 and 7.6 μm) were employed to investigate the effect of BLT on thermal performance. The results from junction temperature measurement show that there is a rapid increase in between 60 and 180 seconds after the power is on for all samples and then systems reached steady-state after 600 seconds when junction temperature remained constant. For WDAA and Ag-DAA with same BLT, the difference in junction temperature at steady-state is about 10℃ and the result indicates that WDAA with 20 μm BLT has larger thermal resistance than Ag-DAA. However for WDAA with 7.6 μm, the junction temperature is only about 74℃ and is 8℃ lower than that of the Ag-DAA sample. The results prove that with thinner BLT, WDAA can show better thermal performance in terms of lower junction temperature at steady-state. Optical and thermal measurements shown in Fig. 5.5 and 5.6 are consistent with each other: first there is a drop in radiation output before 180 seconds, which is due to the rapid increase in junction temperature. Then radiation output becomes steady after 600 seconds when the junction temperature becomes almost constant.

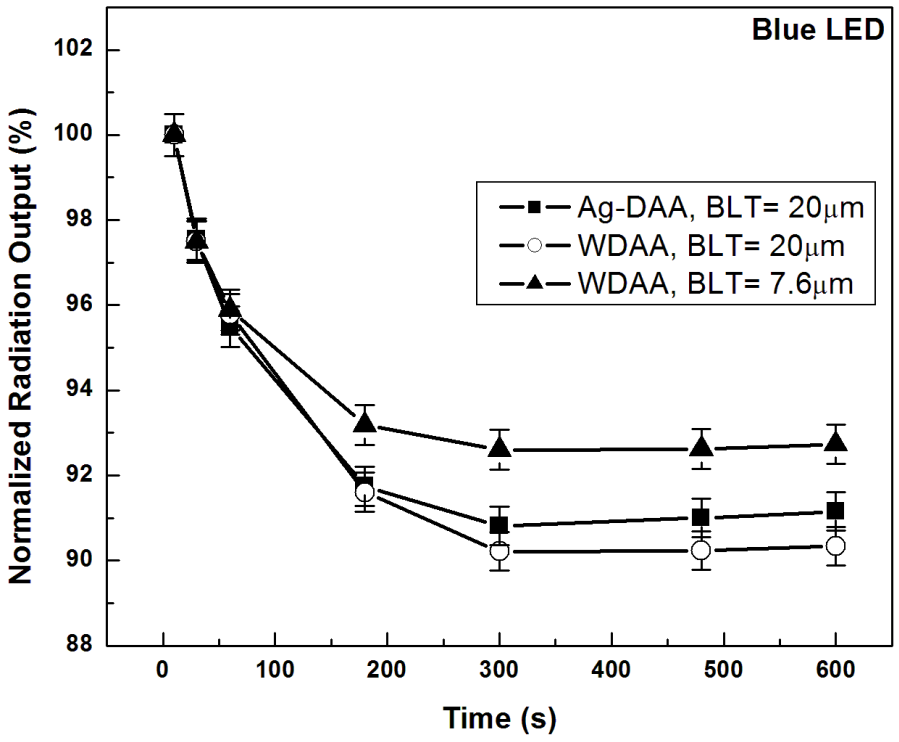

Figure 5.5. Normalized steady-state radiation output of 1 W (I=350 mA and V=3.3 V) monochromatic LED emitters packaged with WDAA and Ag-DAA and encapsulated with silicone, as a function of operation time. All three samples are set as 100% initially.

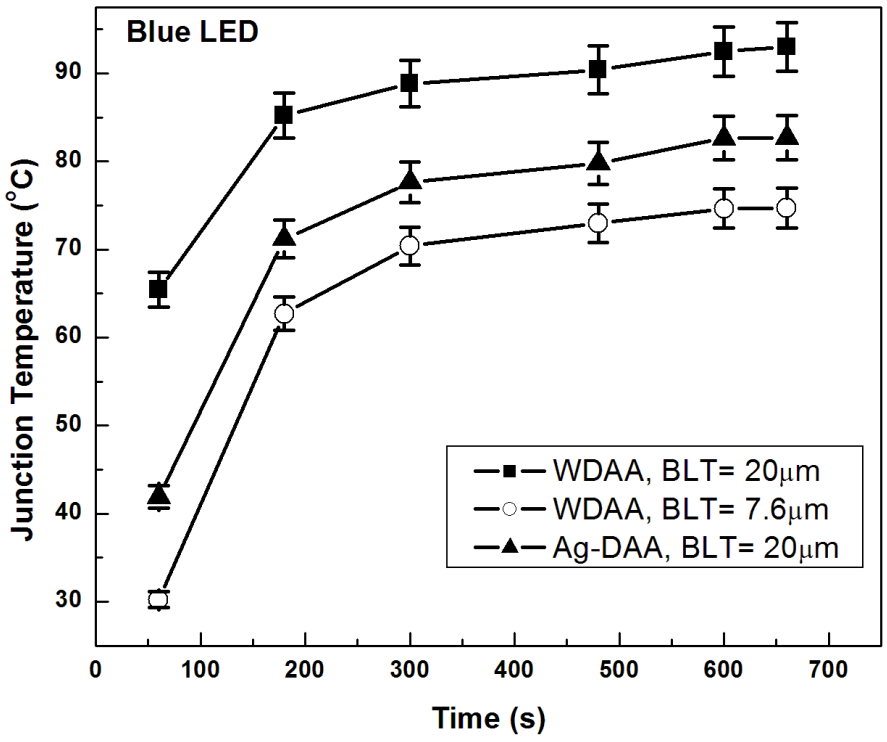

Figure 5.6. Junction temperature of different 1 W (I=350 mA and V=3.3 V) monochromatic LED emitters packaged with different DAA materials and encapsulated with silicone, as a function of operation time.

Figure 5.7 shows the result of the reliability test performed in a temperature-humidity testing chamber, with testing conditions of 80℃ and 85% relative humidity. Fillet coverage for the tested sample is 40% for all tested samples. Input current is 350 mA and the forward voltage is 3.3 V for all samples. This reliability test follows the Joint Electron Devices Engineering Council (JEDEC) 22-A101-B test method and is a steady-state temperature humidity bias life test for the purpose of evaluating the reliability of non-hermetic packaged solid-state device in humid environment [9]. The results show that after 1000-hour testing duration, samples with WDAA remain 99.87% of the initially light output, while Ag-DAA samples only exhibit 97.5% of its initially value. The 0.13% drop in WDAA samples is due to the degradation of the leadframe materials, which is polyphthalamide (PPA) and is of high reliability risk. The extra drop in Ag-DAA samples is from the degradation of epoxy matrix, which has been proven to experience huge loss in the optical properties after 300-hour aging time in the combination of heat and moisture [9]. The increased loss in light output is because the increased absorption of epoxy matrix. However the value is not as high as claimed in the study of encapsulation, which is about 50% and the reason is because the exposed area of DAA layer is less than 5% so the effect is limited on the small surface area [4, 9].

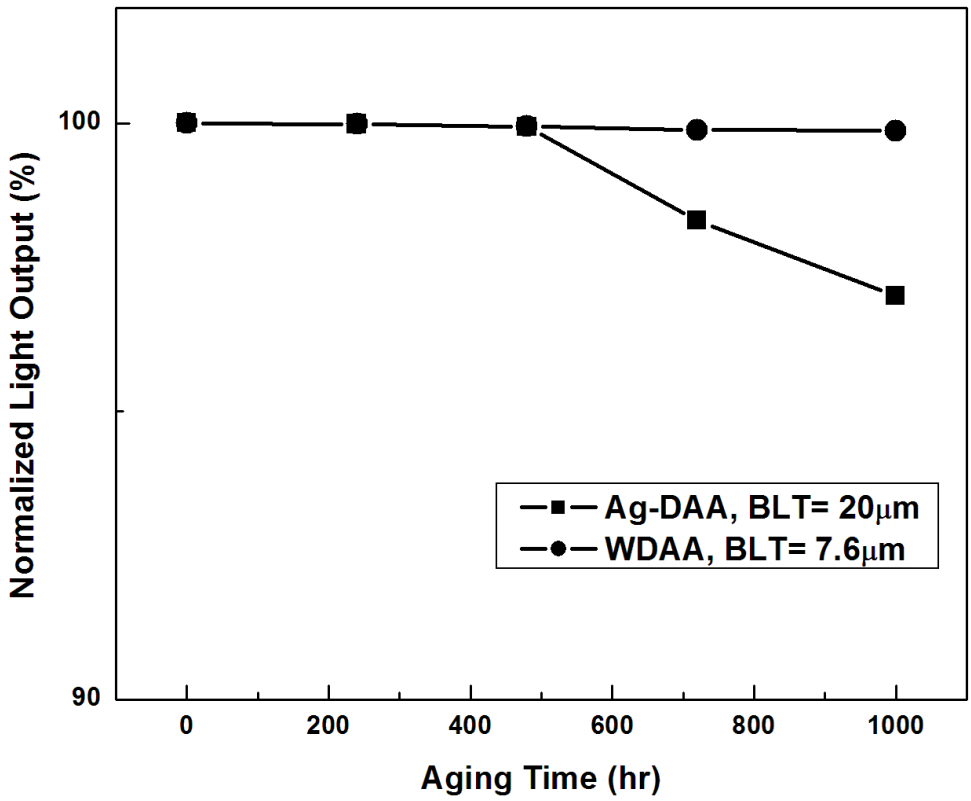

Figure 5.7. Light output degradation of 1 W (I=350 mA and V=3.3 V) monochromatic LED emitters packaged with two different DAA materials and encapsulated with silicone, as a function of aging time. Aging was performed under 85% humidity at 85℃ in the testing chamber.

5.4 Conclusion

In this work, a novel optically reflective die attach adhesive is introduced for LED packaging, and its optical and thermal performance is compared with the conventional silver-filled epoxy die attach adhesive. It is shown that the optically reflective die attach adhesive exhibits better light extraction efficiency, and the result of junction temperature measurement also shows that with a thin bondline thickness, samples packaged with the optically reflective die attach adhesive possesses lower junction temperature and therefore smaller light output degradation during operation. Our studies demonstrate that this novel material can provide outstanding thermal management, as well as excellent light extraction efficiency. This material is also suitable for chip-scale packaging due to the requirement of low fillet coverage in order to maximize the light extraction efficiency. Unlike the conventional silver-epoxy die attach materials, optical reflective die attach adhesive does not suffer from the effect of phosphor back-scattering and therefore the high light extraction efficiency can be maintained for white LED emitters.

References

[1]. P.H. Chen, L.C. Chang, C.H. Tsai, Y.C. Lee, W.C. Lai, M.L. Wu, C.H. Kuo and J.K. Sheu, "GaN-Based Light-Emitting Diodes With Pillar Structures Around the Mesa Region," *IEEE J. Quantum Elect.*, vol. 46, No. 7, pp. 1066-1071 (2010).

[2]. M. Maier, T. Passow, M. Kunzer, W. Pletschen, K. Kohler and J. Wagner, "Towards a deeper understanding of the reduced efficiency droop in low defect-density GaInN wide-well LEDs," *Phys. Status Solidi C*, vol. 7, No. 7-8, 2148-2150 (2010).

[3]. H.J. Chiu, Y.K. Lo, J.T. Chen, S.J. Cheng, C.Y. Lin and S.C. Mou, "A High-Efficiency Dimmable LED Driver for Low-Power Lighting Applications," *IEEE T. Ind. Electron.*, Vol. 57, No. 2, pp. 735-743 (2010).

[4]. Y.C. Shih, G.W. Kim, L.J. Huang, J.P. You and Frank G. Shi, "Role of Transparent Die Attach Adhesives for Enhancing Lumen Output of Mid-Power LED Emitters with Standard MESA Structure," *IEEE Trans Compon. Packag. Manuf. Tech.*, accepted to be published.

[5]. J. Piprek, "Efficiency droop in nitride-based light-emitting diodes," *Phys. Status. Solidi. A*, Vol. 207, No. 10, pp. 2217-2225 (2010).

[6]. D.F. Feezell, J.S. Speck, S.P. DenBaars and S. Nakamura, "Semipolar (20-2-1) InGaN/GaN light-emitting diodes for high-efficiency solid-state lighting," *J. Disp. Technol.*, vol. 9, No. 4, pp. 190-198 (2013).

[7]. N.F. Gardner, G.O. Muller, Y.C. Shen, G. Chen, S. Watanabe, W. Gotz and M.R. Krames, "Blue-emitting InGaN–GaN double-heterostructure light-emitting diodes reaching maximum quantum efficiency above 200A⁄cm^2," *Appl. Phys. Lett.*, 91, 243506 (2007).

[8]. G. Liu, J. Zhang, C.K. Tan and N. Tansu, "Efficiency-droop suppression by using large-bandgap AlGaInN thin barrier layers in InGaN quantum-well light-emitting diodes," *IEEE Photonic. Tech. L.*, vol. 5, No. 2, 2201011 (2013).

[9]. Y.H. Lin, J.P. You, Y.C. Lin, N.T. Tran, F.G. Shi, "Development of high-performance optical silicone for the packaging of high-power LEDs," *IEEE Trans Compon. Packag. Manuf. Tech.*, vol. 33, No. 4, pp. 761-766 (2010).

[10]. B. Yan, J.P. You, N.T. Tran, Y. He, F.G. Shi, "Influence of die attach layer on thermal performance of high power light emitting diodes," *IEEE Trans. Compon. Packag. Manuf. Tech.*, vol. 33, No. 4, pp. 722-727 (2010).

[11]. Y. Shao, Y.C. Shih, G. Kim and F.G. Shi, "Study of optimal filler size for high performance polymer-filler composite optical reflectors," *Opt. Mater. Express*, vol. 5. issue 2. pp. 423-429 (2015).

CHAPTER 6

LIGHT OUTPUT DEPENDENCE ON THE INTERACTION BETWEEN LED CHIP BACKSIDE REFLECTOR AND DIE ATTACH ADHESIVES

6.1 Introduction

Mid-power LED emitters (input power up to 0.8 W), with a MESA structure on a sapphire substrate as illustrated in Fig. 4.1, has dominated the backlighting application for LCD displays and TVs, and its application to general lighting has also seen a significant increase for the last few years [1-5]. It is also expected that mid-power LED emitters will make up about 48 percent of packaged LED emitters in general lighting market in 2014 [3, 5]. Mid-power LED emitters offer the highest performance to cost ratio as well as better light output control in terms of both brightness and uniformity in comparison with high-power LED emitters [5]. For continuing more widely adoption of mid-power LEDs in the general lighting market, the market demands a further cost reduction in LED emitters, as well as a further enhancement in light extraction. One of the recent technologies introduced by the industry is the introduction of backside reflecting layer on the bottom surface of the LED chip [1-7]. Downward emission from the multiple quantum well (MQW) was considered as an important issue at the chip level because a large portion of these photons will be absorbed by the packaging materials, resulting in a lost in the optical output. Integration of a backside reflector (BR) has been found to hugely enhance the light extraction (up to 50%) [1-6]. However, the reported huge enhancement with a

BR by Lin is mainly for naked LED chips without the practical packaging procedure and materials [2, 3]. Firstly, the measurement methods cannot reflect the effect of packaging factors, including the packaging materials, such as the reflector cup and die attach materials (DAAs), and processing conditions. In a practical packaged LED emitter, all these factors, including packaging parameters and selection of materials for each component, should be involved and considered in order to determine the optical performance. Secondly, the compositions of the highly effective backside reflectors introduced in these literatures are very complicated and are not cost-effective in enhancing the optical performance of mid-power LED emitters. Among different types of reflectors, including metallic reflectors, distributed Bragg reflector (DBR), hybrid metal-DBR, total internal reflector (TIR) and the omni-directional reflector, metallic reflectors are still the most common backside reflectors in mid-power LED emitters due to their ease of fabrication and high reflectivity [7]. Thirdly, the metallic compounds used in these reports mentioned above are mainly silver and aluminum [1, 2, 4], instead of gold and gold alloys, such as AuBe. Gold and gold alloys are the most common materials for the metallic reflectors in LED emitters due to their excellent adhesion, processibility and reliability performance, although the reflectance of gold is only about 50% [7]. Silver, despite its high reflectivity (95% at 450 nm) [2], has very poor vulcanization resistance, while the oxidation layer on the aluminum surface is brittle and cause weaker adhesion between the chip and the die bonding material. So both metals alone are not sufficient for being the metallic reflectors in LED emitters. The claimed 50% enhancement by Lin is between a BR-free emitter packaged with epoxy-silver DAA, which shows very high light absorptance [5], and BR-based emitter with a complex BR configuration (Ag + 3 DBR layers) [2]. The difference will not be so significant if a simpler and less reflective reflector is used instead. Moreover, Lin's work shows that with a

complex BR configuration (Ag + 3 DBR layers), the enhancement is only 1% higher than that of the simple Ag BR, which again indicates that the complicated configuration of the BR is totally unnecessary, especially for LED emitters operating with a low input current [2].

In this work, the effectiveness of the Au- and silver-based BR was examined by comparing the light output of leadframe-packaged blue and white LED emitters with and without a BR. Different types of DAAs, including optically clear, reflective and epoxy-silver DAAs were employed and the influence of different DAA materials, as well as DAA fillet coverage, was investigated. We demonstrate that if an optically clear or reflective DAA is applied, the light output of the BR-free chips can be dramatically enhanced and exceed that of chips with an Au-based BR. For the optically clear DAA with 40% fillet coverage, BR-free blue chips show 20% higher light output than BR-based blue chips. If the optically reflective DAA is applied with the same fillet coverage, the difference becomes 22%. The mechanism in enhancing output light with different DAAs is elucidated. For blue chips with an Ag-based BR, the enhancement from BR-free chips is about 4.5% with optically clear DAA at 40% fillet coverage and therefore the result implies that BR-free chips packaged with optically clear DAA can provide a cost-effective method in enhancing the performance/cost ratio of LED packaging.

6.2 Experimental

In this work, commercial available 0.8 W blue emitters with a dominant wavelength at 452 nm were used and were of no backside reflector when received. The Ti/Au and Ag backside reflecting layers were coated by evaporation deposition and the thickness is 20, 130 and 120 nm for titanium, gold and silver, respectively. The packaged 0.8 W blue LED emitter is comprised of a 5050 leadframe (5x5x1.2 mm) with a reflector cup, an LED chip, a die attach adhesive, gold

wires and silicone encapsulant with an index of refraction equal to 1.53. Figure 6.1 illustrates the schematic drawing of a packaged typical 0.8W LED emitter. In order to present each layer more clearly, in Fig. 6.1 (b) layers are not plotted in their relative thickness. The value of thickness of different layers might be varied based on different designs of LED chips. The blue LED emitter used in this work is operated at the constant current mode (I = 220 mA), and the size of the chip is 24x48 mil (0.61x1.22 mm) with a thickness about 150 μm.

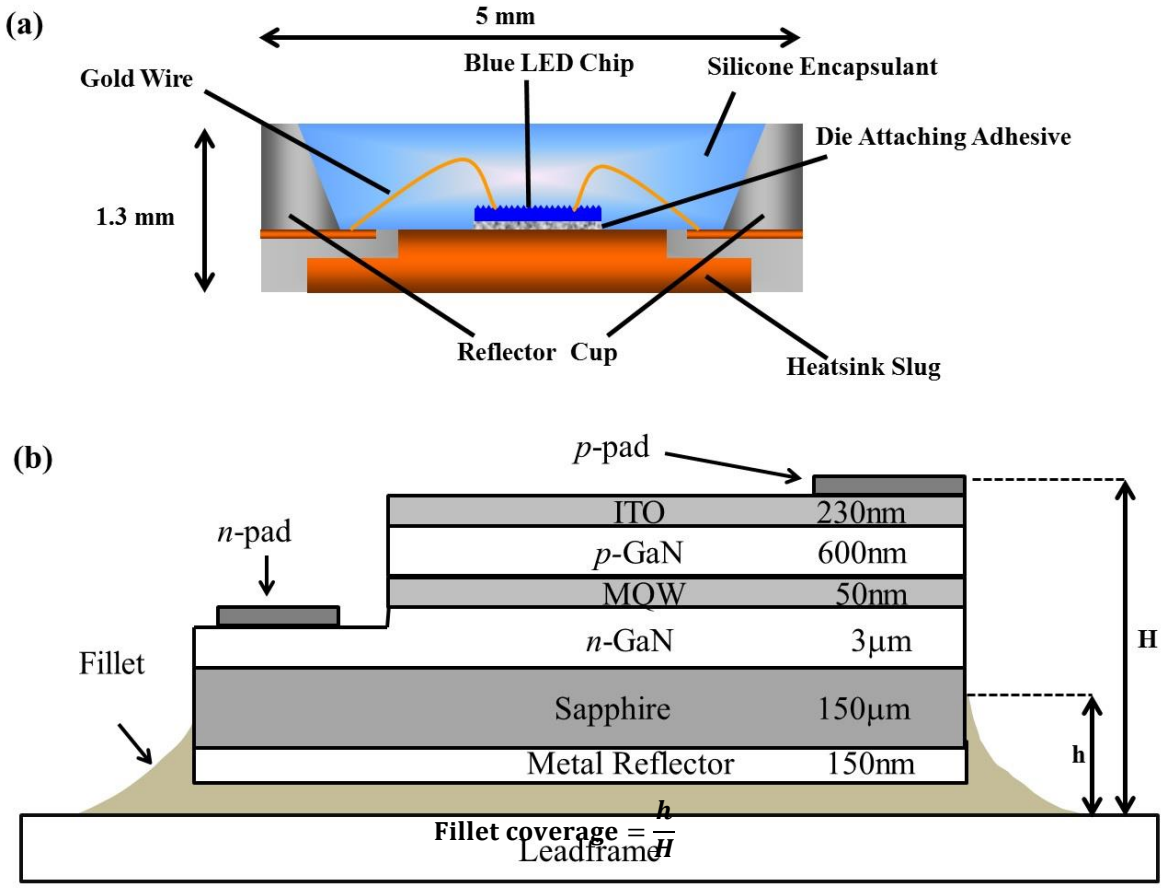

Figure 6.1. (a) Schematic drawing of a cross-sectional view of a 0.8 W monochromatic blue LED package with pure silicone encapsulant; (b) A macroscopic enlargement of the chip and the DAA layer.

Three DAAs were employed in this study. The first one is the optically clear DAA (denoted as OC-DAA), the second one is the optically reflective white DAA (denoted as WDAA) and the third one is the conventional epoxy-silver DAA (denoted as Ag-DAA). The properties of these three DAAs are summarized in Table 6.1. For white LED emitters used in this work, silicone encapsulant mixed with 7.5 wt.% of yellow phosphor powder was used as the encapsulant material and the resulted CCT is about 9200 K. One important parameter for bonding materials is the fillet coverage around the chip, as schematically shown in Fig. 6.1 (b).

Table 6.1. Physical properties of three different DAAs used in this work.

	Appearance	Reflectance @450 nm	Transmittance @450 nm
OC-DAA	Colorless	-	85%
WDAA	White	92%	-
Ag-DAA	Silver	27%	-

Sample thickness: 1mm

The complete packaging process is as follows: (1) the 5050 leadframe (5x5x1.2 mm) used in this experiment is cleaned by isopropyl alcohol and baked at 80 ℃ before used; (2) the 0.8W blue LED chip is attached to the center of the leadframe by used a die attaching adhesive; (3) the samples are then cured at 150 ℃ for 2 hours; (4) wire-bonding is performed to electronically connect the LED chip to the leadframe; (5) silicone encapsulant with and without phosphor is poured into the cavity of the reflective cup to encapsulate the LED chip; (6) the samples then are cured at 150 ℃ for 2 hours; (7) The packaged LEDs are then soldered to Al-based printed-circuit-board (PCB). In order to avoid the image distortion caused by the silicone encapsulant, the measurement of DAA fillet coverage is conducted with an optical microscope after the first curing step listed above.

Power generator by Everfine with constant current mode was used for this work and the value of the current was 220 mA. Light output of packaged LED emitters was measurement in a LabSphere integral sphere. Transmittance in Table 6.1 was measured by GENESYS 20 spectrophotometer by Thermo Electron Corporation, and reflectance in the same table was measurement with IS-1 integrating sphere by Filmetrics. Thickness of samples for both transmittance and reflectance measurement is 1 mm.

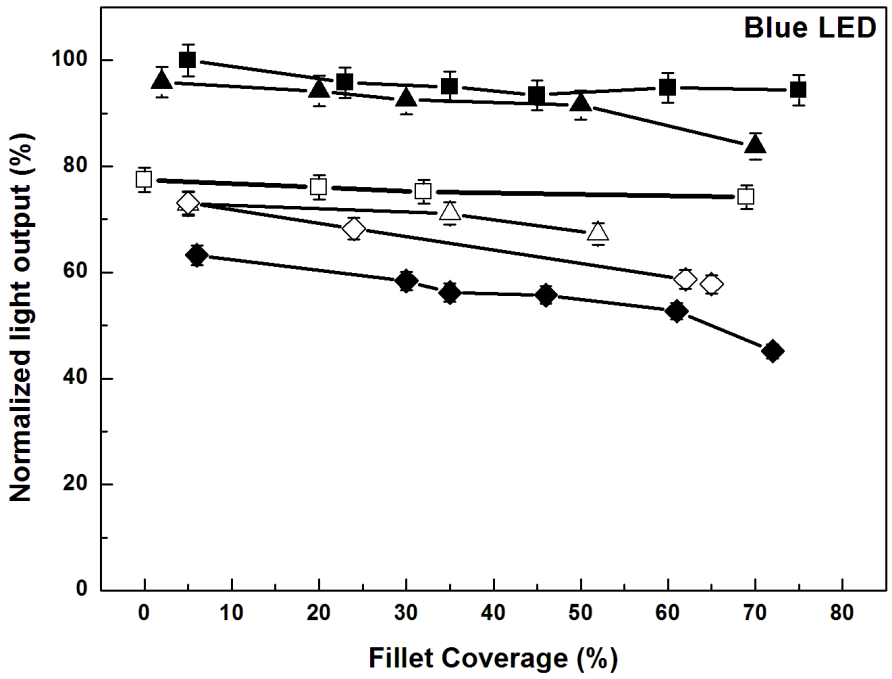

Figure 6.2. Normalized light output of 0.8 W blue LED emitters with and without a Ti/Au BR, as a function of DAA fillet coverage. ■: OC-DAA without a BR, ▲: WDAA without a BR, □: OC-DAA with a BR , △: WDAA with a BR, ◇: Ag-DAA with a BR and ◆: Ag-DAA without a BR.

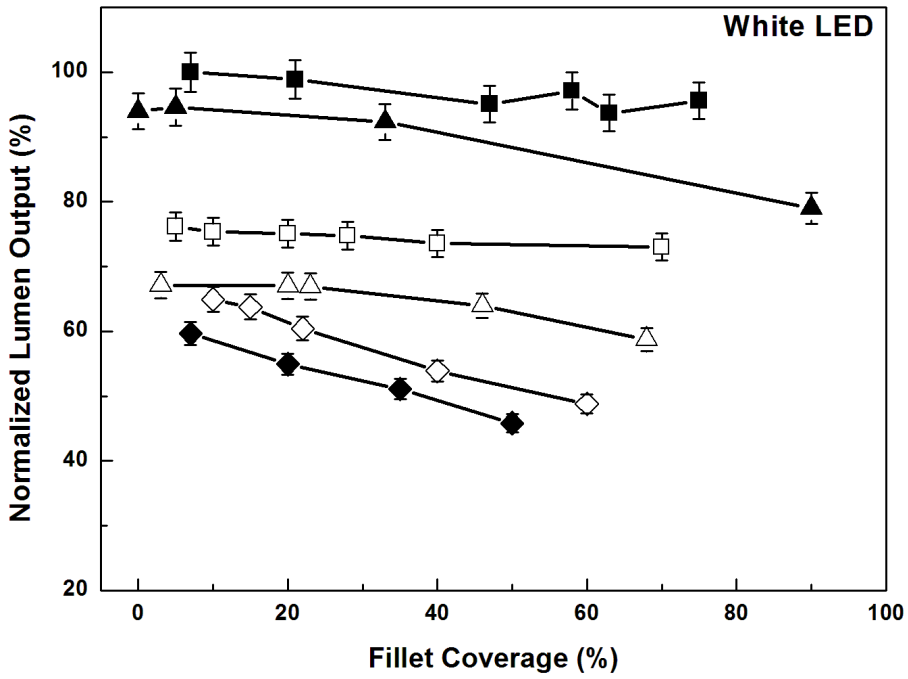

Figure 6.3. Normalized light output of 0.8 W white LEDs with and without a Ti/Au BR, as a function of DAA fillet coverage. ■: OC-DAA without a BR, ▲: WDAA without a BR, □: OC-DAA with a BR , △: WDAA with a BR, ◇: Ag-DAA with a BR and ◆: Ag-DAA without a BR.

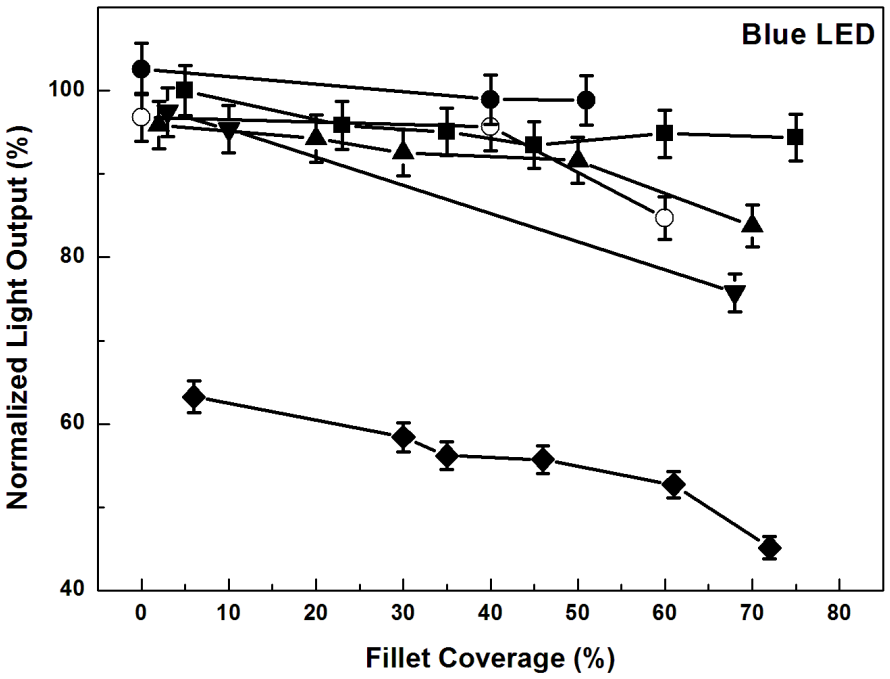

Figure 6.4. Normalized light output of 0.8 W blue LED emitters with and without an Ag BR, as a function of DAA fillet coverage. ■: OC-DAA without a BR, ▲: WDAA without a BR, ●: OC-DAA with a BR , ○: WDAA with a BR, ▼: Ag-DAA with a BR and ◆: Ag-DAA without a BR.

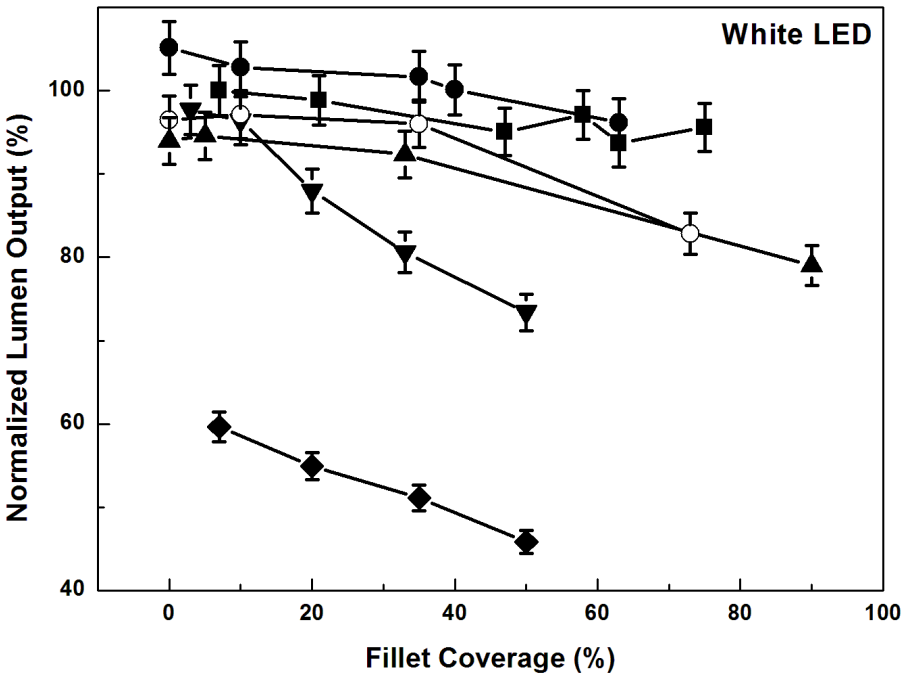

Figure 6.5. Normalized light output of 0.8 W white LEDs with and without an Ag BR, as a function of DAA fillet coverage. ■: OC-DAA without a BR, ▲: WDAA without a BR, ●: OC-DAA with a BR , ○: WDAA with a BR, ▼: Ag-DAA with a BR and ◆: Ag-DAA without a BR.

6.3 Result and Discussion

Figure 6.2 and 6.3 show the normalized optical output of blue and white LEDs, with and without a Ti/Au BR, as a function of fillet coverage with different DAAs. Figure 6.4 and 6.5 show the normalized optical output for blue and white LEDs, with and without an Ag BR, as a function of fillet coverage with different DAAs. In these figures the optical output of BR-free packaged with OC-DAA and lowest fillet coverage is set as 100% as the reference. For both blue and white LED applications, the difference in light output at low fillet coverage is smaller due to less photons are blocked by the DAA layer at the sidewall [5]. In other words, to consider this effect, a die attach film should be more suitable for bonding LED emitters [8].

I. Blue LEDs with a BR

For blue LEDs with a Ti/Au BR, the difference between three DAAs, especially at higher fillet coverage, is due to the photon blocking taking place at sidewall [5]. For samples packaged with WDAA and Ag-DAA, as shown in Fig. 6.2, DAA materials covering the sidewall block incident photons due to the reflecting nature of WDAA and the absorbing nature of Ag-DAA. For samples packaged with WDAA, it is possible that the photons can still propagate through the DAA layer at sidewall after multiple reflection and scattering. However for Ag-DAA, the possibility for photons to propagate through the DAA layer at sidewall is much smaller due to the high absorptance of Ag-DAA. This explains why the decrease in light output of Ag-DAA samples is larger than that of WDAA samples at higher fillet coverage. For samples with low fillet coverage, the difference in light output between different DAAs becomes smaller because smaller portion of LED sidewalls is covered by DAA materials. For samples packaged with OC-

DAA, the change in light output with different fillet coverage is slight because OC-DAA only absorbs a small amount of photons.

For blue LED chips with an Ag BR, the light output is higher than BR-free chips due to the high reflectance of silver reflector, as shown in Fig. 6.4. For samples packaged with OC-DAA, light path in Ag BR-based chips is shorter and the absorption of photons by the DAA materials could be prevented except the section of sidewall. For WDAA samples, because the reflectance of WDAA material is about 3% lower, the light output of BR-free chips is slightly lower than that of Ag BR-based chips. For Ag-DAA samples, because the reflector can effectively reflect photons upward, there is high ratio of absorption at the chip/DAA interface.

II. Blue LEDs without a BR

For blue LEDs without a BR, samples packaged with OC-DAA and WDAA show much higher light output than Au BR-based chips, as shown in Fig. 6.2. In the cases of OC-DAA, the photons propagate through the DAA layer and are reflected by the silver plating on the leadframe. The reflectance of silver plating is more than 90% and is much higher than that of the gold reflector, whose absorptance is about 50% at wavelength equal to 450 nm. Therefore the combination of OC-DAA and BR-free chips has very high optical output and the difference between Au BR-based and BR-free blue LEDs with 40% OC-DAA coverage is 20%. If the Ag BR is used instead, BR-free blue LEDs show 4.5% less light output at 40% fillet coverage. Light output performance of BR-free chips with OC-DAA can be further improved by changing the optical properties of OC-DAA, such as increasing the transmittance to reduce photon absorption, and increasing the refractive index to avoid the total internal reflection at the sidewall, which is

the reason OC-DAA performs better at lower fillet coverage. Thinner bondline thickness can also be applied to reduce the photo absorption.

For BR-free chips packaged with WDAA, the highly reflective DAA material can serve as the reflector with 92% reflectance and therefore BR-free chips have higher light output than Au BR-based chips and only slightly lower than Ag BR-based chips. The improvement with 40% fillet coverage is about 22% between BR-free and BR-based chips. For Ag BR-based chips, the light output is about 3.6% higher than that of BR-free chips. Sidewall blocking of WDAA material is not as significant as Ag-DAA because photons can still escape after multiple scattering inside the WDAA materials. Light output of LED chips packaged with WDAA can be further improved by using WDAA with higher reflectance. Reducing the fillet coverage of WDAA also can provide enhancement in optical output. Because reflection of photons happens at the surface of DAA layer, changing the bondline thickness will not affect the optical performance.

For Ag-DAA, a very large portion of photons will be absorbed at the sapphire/DAA interface. The high absorptance is the nature of epoxy-silver composites so Ag-DAA is not suitable for LED chips without a BR [5]. Because the absorptance of Ag-DAA is higher than the gold reflector, BR-based chips show 9% higher light output than BR-free chips when the fillet coverage of Ag-DAA is 40%. For Ag BR-based chips at low fillet coverage, Ag-DAA can perform almost the same as WDAA but the light output drops rapidly as the fillet coverage increases due to the high absorption of Ag-DAA.

III. White LEDs applications

Figure 6.3 and 6.5 show the normalized lumen output of white LEDs, with and without a BR, as a function of fillet coverage with different DAAs. With 40% fillet coverage in Fig. 6.3, the difference in lumen output between BR-free and Au BR-based chips is 23%, 27% and 13% for OC-DAA, WDAA and Ag-DAA, respectively. The tendency is similar with that of blue LEDs for all three DAAs but the difference between different samples becomes larger. This is because in the cases of white LEDs, the chance of photons to be absorbed increases due to the scattering by the phosphor particle [5, 9, 10]. The back-scattered photons might be absorbed by the chips and DAA materials. This extra loss in white LEDs cases can be improved by using OC-DAA with higher transmittance, WDAA with higher reflectance, and less fillet coverage or film type adhesives to reduce the chance of absorption [5]. In Fig. 6.5, the difference in lumen output between BR-free and Ag BR-based white chips is similar with that of blue chips and the mechanism is same as described above.

IV. Influence of fillet coverage

For all three DAAs, the light and lumen output decreases as fillet coverage increases. This decrease in samples with OC-DAA is slight because OC-DAA is of high transmittance, especially at a thin thickness. For WDAA at low fillet coverage, photons can still propagate through DAA layer after multiple scattering. The loss in light output becomes more significant at higher fillet coverage when the fillet becomes thicker. For Ag-DAA, the loss in light output is huge even at low fillet coverage due to its high absorption. The loss due to fillet blocking or absorption, especially for WDAA and Ag-DAA, can be diminished by using film type adhesives.

6.4 Conclusion

In this work, light output of leadframe-packaged mid-power monotonic and white LED emitters with and without a BR was compared by using three different DAA materials with different fillet coverage. It is found that mid-power LED emitters without a backside reflector can still perform high light output efficiency when optically clear and reflective DAAs are used. The backside reflectors become less important with these two types of DAAs, especially at low fillet coverage. For the consideration of cost-efficiency and production rate, it is logical to skip the deposition of backside reflector layers, especially for mid-power LED emitters. With the ongoing improvement on the bonding materials, it is possible that LEDs without backside reflector can reach the same light extraction efficiency as LEDs with backside reflector. Film-typed adhesives also become valid options to eliminate the sidewall effect of DAAs and can be integrated into chip scale packaging (CSP) for more efficient production.

References

1. H. Guo, X. Zhang, H. Chen, P. Zhang, H. Liu, H. Chang, W. Zhao, Q. Liao, Y. Cui, "High performance GaN-based LEDs on patterned sapphire substrate with patterned composite SiO_2/Al_2O_3 passivation layers and TiO_2/Al_2O_3 DBR backside reflector", *Opt. Express*, vol. 21, No. 18, pp. 21456-21465 (2013).
2. N.M. Lin, S.C. Shei, S.J. Chang, "Nitride-Based LEDs With High-Reflectance and Wide-Angle Ag Mirror+SiO_2/TiO_2 DBR Backside Reflector", *J. Lightwave Technol.*, vol. 29, No. 7, pp. 1033-1038 (2011).
3. G. Kim, Y.C. Shih, N.T. Tran, J.P. You, F.G. Shi, *IEEE Photonic. Tech. L.*, submitted for publication.
4. H. Chen, H. Guo, P. Zhang, X. Zhang, H. Liu, S. Wang, Y. Cui, "Enhanced Performance of GaN-Based Light-Emitting Diodes by Using Al Mirror and Atomic Layer Deposition-TiO2/Al2O3 Distributed Bragg Reflector Backside Reflector with Patterned Sapphire Substrate", *Appl. Phys. Express*, vol. 6, pp. 022101 (2013).
5. Y.C. Shih, G. Kim, L. Huang, J.P. You, F.G. Shi, *IEEE Trans. Compon. Packag. Manuf. Tech.*, submitted for publication.
6. L.C. Chen, H.C. Feng, "Improved performance of InGaN/GaN blue light-emitting diodes with a SiO_2/TiO_2 Bragg reflector", *Phys. Stat. Sol. (a),* vol. 202, No. 14, pp. 2836-2839 (2005).
7. E.F. Schubert, *Light-Emitting Diodes*. 2nd ed., New York: Cambridge University Press, 2006, ch. 10, pp. 163-168.
8. V.R. Manikam, K.Y. Cheong, "Die Attach Materials for High Temperature Applications: A Review", *IEEE Trans. Compon. Packag. Manuf. Tech.*. vol. 1, No. 4, pp. 457-478 (2011).

9. N. Narendran, Y. Gu, J.P. Freyssinier-Nova, Y. Zhu, “Extracting phosphor-scattered photons to improve white LED efficiency”, *Phys. Stat. Sol. (a)*, 202, No. 6, pp. R60-R62 (2005).
10. S.L. Hsiao, N.C. Hu, H. Cornelissen, “Phosphor-converted LED modeling using nearfield chromatic luminance data”, *Opt. Express*, vol. 21, issue S2, pp. A250-A261 (2013).

CHAPTER 7

SUMMARY AND CONCLUSIONS

In the first chapter of this dissertation, a brief introduction is given for two optoelectronic devices, solar cells and light-emitting diodes, which now extensively used in daily applications. Basic and fundamental theories and mechanism about the operation of these two optoelectronic devices are introduced. Although the two devices operate in opposite mechanisms, we are facing the same issues associated with performance/cost ratio, overall efficiency and thermal management in order to achieve better quality of services.

In chapter 2, a study of size effect on etching ability of ceramic additives in screen-printable silver paste for crystalline silicon solar cells shows that with nano-sized additives, a device with low specific contact resistivity could be achieved due to the low amount of residual glass layer at the interface between front silver electrodes and the *n*-type silicon emitting layer. This is a direct result of excellent etching ability possessed by nano-sized additives due to the larger surface area per unit mass. Samples made by nano-sized glass frits show specific contact resistivity only 40% of that from micro-sized glass frits with their optimal firing conditions. The results from this chapter demonstrate the importance of nanomaterials for application involved with chemical reaction.

In chapter 3, the surface property of nano-sized ceramic additives is further improved by coating a thin silver layer on the surface of the additives via electroless plating. Electroless plating enables the additives to carry a partially covered silver coating, which acts as a blocker between two adjacent isolating particles and ensures the resultant glass residuals are discrete and the clusters are smaller. This result further improves the specific contact resistivity by 24% with

otherwise identical conditions. This work proofs that surface modification via electroless silver plating on nano-sized ceramic additives can provide a promising technology to further improve the electrical performance of silicon solar cells.

Beginning from chapter 4, the focus is now on LED applications. In chapter 4 the optical impact on light extraction efficiency of packaged LED emitters with different types of die attach adhesives is investigated for the first time. The result shows that such an optical impact is enormous when the optical clear adhesive is employed, we can achieve an optical output 21% more than the conventional silver-filled epoxy adhesive. This improvement comes from low light absorptance of the optical clear material. From the junction temperature measurement, it is proven that for mid-power LEDs, the optical clear die attach adhesive is sufficient for thermal management even it has a lower thermal conductivity. The effect of fillet coverage is also investigated and the result indicates that due to the side-wall blocking, film type adhesives will be better choices in term of optical performance.

In chapter 5 a novel optically reflective die attach adhesive is developed and tested. The result shows that with this new material, light extraction efficiency is much higher than the conventional epoxy-based silver die attach adhesives, while their mechanical performance is similar. When a thin bondline thickness is applied with the optically reflective die attach adhesive, the thermal performance exceeds that of the conventional one. This study demonstrates that this new material can provide outstanding thermal management and excellent light output performance.

The last part focus on the interface between LED chips and the die attach adhesives. We demonstrated for the first time that with optical clear die attach materials, the silver plating on leadframe can replace the backside reflector, which is of high cost and also involves complex

processes. When the reflective white die attach adhesive is applied with LED chips without backside reflectors, the light extraction efficiency is also high, especially with low fillet coverage. With these two types of die attach adhesives, backside reflectors become less important and for the consideration of cost-efficiency and production rate, it is reasonable to skip the deposition of backside reflectors. Again low fillet coverage is found to beneficial with LED chips without backside reflectors so the integration of film-type adhesives with chip scale packaging can provide more efficiency to the manufacturing.